Research Square

Preprints are preliminary reports that have not undergone peer review.
They should not be considered conclusive, used to inform clinical practice,
or referenced by the media as validated information.

Extracellular vesicle-associated α-synuclein disrupts retrograde signalling-endosome trafficking in recipient neurons

Frédéric Meunier

f.meunier@uq.edu.au

Clem Jones Centre for Ageing Dementia Research, Queensland Brain Institute, The University of Queensland, Brisbane, QLD, 4072, Australia and School of Biomedical Sciences, The University of Queensla https://orcid.org/0000-0001-6400-1107

Barbara Duda

Clem Jones Centre for Ageing Dementia Research (CJCADR), Queensland Brain Institute, The University of Queensland

Saber Saber

The University of Queensland

Vanessa Lanoue

University of Queensland

Raluca Ghebosu

Australian Institute for Bioengineering and Nanotechnology (AIBN)

Adekunle Bademosi

University of Queensland https://orcid.org/0000-0001-5157-8572

Rachel Gormal

The University of Queensland https://orcid.org/0000-0003-1604-0253

Benjamin Matthews

Clem Jones Centre for Ageing Dementia Research (CJCADR), Queensland Brain Institute, The University of Queensland

Tristan Wallis

Clem Jones Centre for Ageing Dementia Research, Queensland Brain Institute, The University of Queensland, Brisbane, QLD, 4072, Queensland, Australia. https://orcid.org/0000-0002-6515-9157

Alex McCann

Clem Jones Centre for Ageing Dementia Research (CJCADR), Queensland Brain Institute, The University of Queensland https://orcid.org/0000-0002-2984-5782

Yara Abosnwber

Clem Jones Centre for Ageing Dementia Research (CJCADR), Queensland Brain Institute, The University of Queensland

Justin Cooper-White
The University of Queensland https://orcid.org/0000-0002-1920-8229
Patrik Verstreken
VIB-KU Leuven Center for Brain & Disease Research, 3000 Leuven, Belgium and KU Leuven, Department of Neurosciences, Leuven Brain Institute, 3000 Leuven, Belgium
Jereme Spiers
The Australian National University https://orcid.org/0000-0001-5872-8983
Natasha Vassileff
The Australian National University
Will Anderson
Centre of Personalized Nanomedicine
Aditya Krishnakumar
Centre of Personalized Nanomedicine
Fiach Antaw
University of Queensland https://orcid.org/0000-0002-2895-3298
Matt Trau
The University of Queensland https://orcid.org/0000-0001-5516-1280
Joy Wolfram
The University of Queensland https://orcid.org/0000-0003-0579-9897

Article

Keywords: α-Synuclein, Conditioned Medium, Axonal Retrograde Transport, Parkinson's Disease, Exosome, Super Resolution Microscopy

Posted Date: August 14th, 2026

DOI: https://doi.org/10.21203/rs.3.rs-10572966/v1

License: This work is licensed under a Creative Commons Attribution 4.0 International License.
Read Full License

Additional Declarations: There is **NO** Competing Interest.

Abstract

α-Synuclein (α-syn) transfer between neurons is increasingly implicated in the spread of synucleinopathies, yet its functional impact on recipient neurons remains poorly defined. Here, using microfluidic chamber technology, we show that conditioned medium from α-syn^{WT}-GFP-expressing donor hippocampal neurons, but not Parkinson's disease mutant α-syn^{A30P} or EGFP controls, selectively reduced the flux of retrogradely transported cholera toxin B-positive carriers in recipient axons. A similar reduction was observed with conditioned medium from neurosecretory PC12 cells co-expressing α-syn^{WT}-GFP and the chaperone HSP90^{WT}, but not the HSP90^{MD7} mutant that disrupts multivesicular body fusion. This effect was prevented by inhibiting dynamin-dependent endocytosis, but not by immunodepletion of soluble α-syn, consistent with uptake of extracellular vesicle (EV)-associated α-syn. Accordingly, isolated EVs from α-syn^{WT}-GFP-expressing PC12 cells contained α-syn. Single-molecule imaging further detected EV-transmitted α-syn^{WT} in recipient axons, where it exhibited reduced mobility and periodic nanoscale clustering relative to α-syn^{A30P}. Together, these findings identify EV-associated α-syn^{WT} as a modulator of retrograde axonal trafficking.

Introduction

Neurons rely on the precise integration of extracellular signals and intracellular transport processes to maintain survival and function over extended timescales. A critical component of this process is the retrograde transport of signalling endosomes, which carry neurotrophic cues from synaptic terminals to the soma and are essential for neuronal maintenance[1–4]. Disruption of these pathways is increasingly recognised as a key feature of neurodegenerative diseases, where defects in axonal transport and synaptic signalling contribute to neuronal vulnerability[1–4].

A defining pathological hallmark of Parkinson's disease (PD) and related synucleinopathies is the accumulation and spread of α-synuclein (α-syn) aggregates across interconnected brain regions[5–7]. The hypothesis that α-syn pathology propagates in a prion-like manner gained support following the observation of host-to-graft transmission in PD patients, where Lewy body-like inclusions developed in transplanted neurons years after implantation[8]. Subsequent *in vitro* and *in vivo* studies confirmed that pathological α-syn can spread between cells and induce neurodegeneration[9–13], with brain-derived α-syn capable of seeding pathology when introduced into animal models[14–17]. Together, these findings established α-syn as a transmissible pathogenic protein that contributes to disease progression.

α-Syn is a presynaptic protein that is enriched at neuronal terminals[18–20] and exists in multiple conformational states, ranging from monomers to higher-order assemblies[21–24]. While several mechanisms for α-syn transmission have been proposed[25,26], EVs have emerged as a particularly compelling pathway. EVs, including exosomes, mediate intercellular communication by transporting cytosolic proteins, lipids and nucleic acids[27,28] from cell to cell. They are generated through the inward budding of endosomal membranes to form intraluminal vesicles thereby transforming the endosomes

into multivesicular bodies (MVBs). MVBs can undergo fusion with the plasma membrane and release these intraluminal vesicles as EVs [28,29]. Early studies demonstrated that EV-associated α-syn can be transferred between cells and induce toxicity[30,31], and subsequent work showed that EVs derived from patient brain tissue can transmit α-syn pathology *in vivo*. In addition, levels of EV-associated α-syn in biological fluids correlate with disease progression in PD[32–34], supporting their relevance in human disease.

Despite this progress, two key questions remain unresolved. Firstly, the mechanisms regulating EV-mediated α-syn release and uptake are incompletely defined. Secondly, and more critically, the functional consequences of α-syn transfer on recipient neurons remain poorly understood. While EV-associated α-syn is often considered in the context of pathological spread, whether it actively alters intracellular processes such as trafficking or signalling has not been investigated.

Here, we test the hypothesis that EV-mediated transfer of α-syn directly altering retrograde trafficking pathways. Building on our previous work demonstrating that presynaptic activity regulates the retrograde flux of autophagosomes and signalling endosomes[1,2], we here examined how EVs containing α-syn influences these processes in recipient neurons. Using microfluidic systems to isolate axonal compartments, we show that conditioned medium from neurons expressing α-syn^{WT}, but not the PD-associated mutant α-syn^{A30P}, selectively and significantly reduces retrograde transport. We further demonstrate that this effect depends on Hsp90-mediated EV release from donor neurons and dynamin-dependent uptake from recipient neurons, linking α-syn transmission to defined vesicular pathways[35]. Finally, using single-molecule super-resolution microscopy, we characterise the intracellular behaviour of transmitted α-syn and reveal a periodic nanoscale organisation in recipient axons.

Together, these findings establish a mechanistic link between EV-mediated α-syn propagation and neuronal trafficking, providing new insight into how transmitted α-syn^{WT} impacts axonal trafficking in recipient neurons, an effect that is completely absent from transmitted disease mutant α-syn^{A30P} suggestive of a loss for function in synucleinopathies.

Results

Extracellular α-syn selectively impairs retrograde axonal transport

To examine the impact of transmitted α-syn on synaptic trafficking, we expressed α-syn-GFP in hippocampal neurons (DIV12), harvested their media after 24 h and applied it onto untransfected (naïve) hippocampal neurons (DIV13) cultured in microfluidic chambers allowing separation of the cell body from nerve terminals to study axonal transport[36]. To test whether such conditioned medium could affect presynaptic trafficking and axonal transport involved in neuronal survival, we used Cholera toxin subunit B (CTB) conjugated to Alexa Fluor™ 555 (CTB-Af555), which was previously shown to be taken up at the

presynapse and transported via long range retrograde axonal transport to the cell body within signalling endosomes[2].

The conditioned medium from the soma chamber was applied to the nerve terminal chamber of the microfluidic device containing naïve neurons with a 70:30 vol/vol ratio (Fig. 1A). The conditioned medium was removed after 24 hours and CTB-Af555 (50 ng/mL) was added for 5 minutes to the nerve terminal chamber in high potassium (56 mM, HK^+) buffer to stimulate post-neuroexocytic uptake of CTB in nerve terminals[1]. Chambers were then washed three times in low potassium (5.6 mM, LK^+) buffer and the conditioned medium was added back (chased) for another 2 hours at 37°C. The number of CTB-positive (CTB+) carriers undergoing fast retrograde axonal transport was examined by time-lapse spinning disk confocal imaging of axons located in microgroove channels. In recipient (untransfected) neurons exposed to conditioned medium from α-syn^{WT}-GFP-expressing neurons, we observed a significant decrease in the number of CTB+ carriers undergoing retrograde transport per second compared with neurons exposed to conditioned medium from neurons expressing EGFP (Fig. 1B and C). This suggests that the conditioned medium from α-syn^{WT}-GFP-expressing neurons can negatively regulate the frequency of signalling endosomes that are transported from the presynapse to the cell body carrying the survival signal. This regulation is likely capable of controlling the number of signalling endosomes, bearing BDNF receptor TrkB, that are transported to the cell body. Indeed, the colocalisation percentage of CTB with TrkB-positive carriers was largely increased in axons that were preincubated with conditioned medium from neurons expressing α-syn^{WT}-GFP, compared to conditioned medium from neurons expressing EGFP (Supp Fig. 1A and B). No difference was observed between conditions for the colocalisation of CTB with LC3-positive carriers (Supp Fig. 1C and D) suggesting that CTB selectively labelled signalling endosomes and not autophagosomes as previously reported[1,2]. We next examined whether the human PD-associated mutation A30P had similar effect on CTB retrograde transport. Interestingly, the conditioned medium from α-syn^{A30P}-GFP expressing neurons did not significantly impact CTB-Af555 retrograde trafficking, suggesting that the PD-linked mutation prevented this regulatory mechanism from occurring. Interestingly, in those axons the percentage of colocalisation between CTB with TrkB-positive carriers was largely decreased compared to neurons preincubated with conditioned medium from neurons expressing α-syn^{WT}-GFP (Supp Fig. 1B). We also asked whether the conditioned medium from α-syn^{WT}-expressing neurons could affect the frequency of CTB+ carriers when applied on the soma chamber of the recipient microfluidic device. However, no effect was observed (Fig. 1D, E and F), suggesting that the conditioned medium acted primarily on presynapses.

Trafficking defects depend on Hsp90-regulated EV release

Since exosomal transmitted α-syn has been implicated in neuronal death[31,37], we reasoned that the effect of α-syn^{WT} conditioned medium could be mediated by the release of α-syn located in exosomes following the fusion of MVBs with the plasma membrane. To visualise exosomal release, we used a common exosomal marker, CD63, coupled to a pH sensitive green fluorescent protein reporter, pHluorin,

which fluoresces only in a neutral environment, namely when exosomes are released from the acidic environment of the intraluminal MVB into the extracellular space[38–40]. We transfected neurosecretory pheochromocytoma (PC12) cells with CD63-pHluorin and used Total Internal Reflection Fluorescence (TIRF) microscopy to image single exocytic events, as previously described[39]. Live imaging of exosomal release was visualised as discrete bursts in fluorescence intensity detected at the plasma membrane (Fig. 2A-E). Secretagogue stimulation using barium chloride promoted an increase in the number of exosomal release events (Fig. 2C). The duration of the fusion 2 D). Recently, the Heat Shock Protein 90 (Hsp90), a chaperone protein, was shown to control the fusion of MVBs with the neuronal plasma membrane, leading to the release of exosomes[35]. Hsp90^{MD7}, bearing 3 substitutions in its amphipathic helix, was uncovered in a screen for *Drosophila* proteins able to deform membranes, and was found to prevent the fusion of MVBs with the plasma membrane (Fig. 2F)[35]. Co-transfection of PC12 cells with CD63-pHluorin and Hsp90^{MD7}-mCherry significantly decreased the number of fusion events observed upon stimulation (68.25% decrease) compared to cells co-transfected with Hsp90^{WT}-mCherry (Fig. 2G), thereby confirming the ability of Hsp90^{MD7} to significantly decrease exosomal release from MVBs[35]. Further, the duration of the detected exocytic events was not sensitive to Hsp90^{MD7} mutation (average of 35.57 seconds and 49.36 seconds for Hsp90^{WT} and Hsp90^{MD7} co-transfected cells respectively), suggesting that the few exocytic events detected were full and complete (Fig. 2H).

Having demonstrated that Hsp90^{MD7} mutations can decrease exosomal release from PC12 cells, we reasoned that co-expression of Hsp90^{MD7}-mCherry with α-syn^{WT}-GFP in these cells could reduce α-syn exosomal release and as a result, impact retrograde trafficking in recipient neurons incubated with the conditioned medium from the PC12 cells (70/30 vol/vol). To test this, we harvested conditioned media from PC12 cells co-transfected with either Hsp90^{WT}-mCherry or Hsp90^{MD7}-mCherry, in combination with either EGFP, α-syn^{WT}-GFP or α-syn^{A30P}-GFP and applied the conditioned media to the NTC of recipient neurons to assess their effect on the retrograde transport of CTB (Fig. 2I). As anticipated, the decrease in the number of CTB+ carriers retrogradely transported in axons incubated with conditioned medium generated in α-syn^{WT}-GFP/Hsp90^{WT}-mCherry co-expressing PC12 cells was lost and returned to control levels (EGFP/Hsp90^{WT}) in axons incubated with α-syn^{WT}/Hsp90^{MD7} conditioned medium (Fig. 2J-K). This result demonstrates that the downregulating effect of α-syn^{WT} conditioned medium on retrograde trafficking requires Hsp90-dependent exosomal release from donor cells. Interestingly, α-syn^{A30P}/Hsp90^{MD7} conditioned medium did not impact axonal transport (Fig. 2K). This suggests that the lack of downregulating effect of α-syn^{A30P} conditioned medium on retrograde transport does not stem from an altered exosomal release. The downregulating effect of conditioned medium from α-syn^{WT}-GFP expressing neurons is therefore likely to be mediated by exosomal α-syn^{WT}.

As α-syn is known to be secreted either as free membrane-less monomers/aggregates[41–43] or within different vesicles[44,45], we reasoned that removing the free forms of α-syn^{WT}-GFP should not impact on the ability of the conditioned medium to downregulate axonal retrograde transport. To test this

hypothesis, we immunodepleted α-syn^{WT}-GFP from the conditioned medium of PC12 cells co-transfected with α-syn^{WT}-GFP and Hsp90^{WT}-mCherry using anti-GFP trap beads (Supp Fig. 2A). We first checked that the conditioned medium was depleted of α-syn^{WT}-GFP by Western Blot. As expected, α-syn-GFP was detected in the original conditioned medium and in the immunoprecipitated bead fraction (Supp Fig. 2B). Interestingly, we could not detect α-syn-GFP in the flowthrough suggesting that the secreted form consists primarily of free α-syn monomers/aggregates. The original and immunodepleted and conditioned media were consequently applied onto the nerve terminal chamber of microfluidic devices (70/30 vol/vol) seeded with naïve hippocampal neurons. After a 24-hour incubation with the conditioned media and a 5-minute pulse with CTB-Af555 diluted in HK^{+} buffer, devices were washed three times with LK^{+}. Neurons were then incubated in the conditioned media for 2 hours before performing timelapse imaging of CTB+ carriers undergoing retrograde transport in axons of the recipient neurons. As anticipated, the number of CTB+ carriers retrogradely transported in recipient neurons incubated with the α-syn^{WT}-GFP immunodepleted conditioned medium from α-syn^{WT}-GFP/Hsp90^{WT}-mCherry co-expressing cells did not statistically change from the number of CTB carriers observed in neurons incubated with the original conditioned medium. Further, this was still significantly lower compared to the number of carriers in neurons incubated with conditioned medium from PC12 cells co-expressing α-syn^{WT}-GFP/ Hsp90^{MD7}-mCherry (Supp Fig. 2C). These results suggest that the exosomal form of α-syn is relatively minor but plays a key role in downregulating retrograde trafficking in recipient neurons.

To verify that α-syn^{WT}-GFP was indeed released following MVB fusion events, we carried out further experiments in hippocampal neurons using CD63-pHuji (red fluorescent version of pHluorin) as an exosomal fluorescent marker. The goal was to visualise α-syn-GFP release from MVBs by assessing the change in fluorescence in the green and red channels in neurons transfected with CD63-pHuji and either EGFP, α-syn^{WT}-GFP, or PD-linked mutant α-syn^{A30P}-GFP (Supp Fig. 3A-C). We detected CD63-pHuji exocytic events in the red channel on the cell body of hippocampal neurons, that were typically characterised by a rapid drop in fluorescent intensity (Supp Fig. 3B-D). This was associated in 40% of the cases with a slow increase in α-syn^{WT}-GFP as observed in the green channel (Supp Fig. 3B, C and E) reflecting the slow release of α-syn^{WT}-GFP containing exosomes. The number of fusion events was increased upon depolarisation with high K^{+} buffer (Supp Fig. 3F) paralleling the effect detected in PC12 cells (Fig. 2C). Interestingly, there was no statistical difference between α-syn^{WT} and α-syn^{A30P} release events in terms of the number of fusion events, the percentage of events containing α-syn-GFP or changes in fluorescence intensity, suggesting that both WT and mutant forms of α-syn were released equally following MVB fusion with the plasma membrane (Supp Fig. 3F-H).. This raises the question of the mechanism underlying the negative regulation of vesicular trafficking by conditioned medium from α-syn^{WT}-GFP expressing neurons.

EV uptake requires dynamin-dependent endocytosis

Considering that the conditioned medium from α-syn^{A30P}-GFP expressing neurons had no impact on retrograde trafficking, and that its exosomal release from donor neurons was equivalent to that of α-syn^{WT}-GFP (Supp Fig. 3), we reasoned that these effects could stem from the differential uptake of α-syn^{WT}-GFP or α-syn^{A30P}-GFP in recipient neurons. The uptake in neuroblastoma cells of exosomes isolated from patients with Lewy Body Dementia, is energy dependent and mediated by dynamin-dependent endocytosis[46]. Furthermore, the integrity of exosomes is essential for the uptake of exosomal α-syn[31,47]. We therefore used a selective dynamin inhibitor, Dyngo®4a, known to block the major types of endocytosis in neurons[48–50], to test whether the negative regulation of axonal retrograde transport afforded by the conditioned medium was sensitive to dynamin inhibition in recipient neurons. We transfected hippocampal donor neurons with either α-syn^{WT}-GFP or α-syn^{A30P}-GFP and harvested the conditioned medium after 24 hours. Recipient neurons from the nerve terminal chamber were incubated in the harvested conditioned medium in the presence of Dyngo4a® (Fig. 3A-B) for another 24 hours. Following a brief wash with fresh conditioned medium to remove the dynamin inhibitor, we pulsed the nerve terminal chamber with CTB-Af555 diluted in HK^{+} buffer for 5 minutes, washed the chamber three times with LK^{+} buffer and replaced the conditioned medium for a 2-hour chase at 37°C. Timelapse imaging and quantification of CTB-Af555 retrograde transport in the axons of the recipient neurons was then performed (Fig. 3A-C). The number of CTB+ carriers was increased in recipient neurons exposed to α-syn^{WT}-GFP conditioned medium and Dyngo®4a compared to neurons exposed to α-syn^{WT}-GFP conditioned medium only, demonstrating that the downregulation of retrograde trafficking relies on dynamin-dependent endocytosis (Fig. 3C). The conditioned medium from the PD-linked mutant α-syn^{A30P}-GFP was used as a negative control, as it did not downregulate retrograde trafficking (Fig. 3C and Fig. 1B-C). Our findings demonstrate that dynamin-dependent endocytosis is required in nerve terminals in order for α-syn^{WT}-GFP conditioned medium to be able to downregulate retrograde trafficking in recipient neurons.

Purification and validation of α-syn-containing extracellular vesicles from donor cells

To biochemically validate vesicular α-syn release in our donor-cell paradigm, we isolated extracellular vesicles (EVs) from the conditioned medium of transfected PC12 cells by sequential clarification and size-exclusion chromatography, yielding an EV-enriched fraction for downstream analyses (Fig. 4A). Cryo-electron microscopy revealed intact, bilayer membrane-bound vesicles, with the expected morphology of small EVs (Fig. 4B). Quantification of the vesicle diameter showed that EVs derived from PC12 expressing GFP alone, or α-syn^{WT}-GFP (control) cells, were of comparable size, with no significant difference between the two groups. Consistent with this, nanoparticle tracking analysis demonstrated a similar size distribution, modal size (most frequently occurring size) and particle number in both control and α-syn-GFP EV preparations (Fig. 4C), indicating that α-syn-GFP expression did not markedly alter EV release or gross vesicle characteristics.

The identity and purity of the isolated EVs were further confirmed biochemically. Immunoblotting showed enrichment of the EV-associated markers CD81 and ALIX in the EV fractions, whereas the endoplasmic reticulum marker calnexin was detected in cell lysates but was absent or strongly depleted in EV preparations (Fig. 4D). Mass spectrometry proteomics analysis similarly detected the canonical EV markers CD81 and CD9 in EV fractions, while calnexin and calreticulin were predominantly associated with whole-cell lysates and showed minimal representation in the purified EV samples (Fig. 4E). Importantly, α-syn-GFP was detected in lysates from PC12-α-syn^{WT}-GFP transfected cells and was also present in the corresponding EV fraction, as shown by both mass spectrometry and immunoblotting, whereas EVs from GFP control cells showed no α-syn signal (Fig. 4F). Together, these findings confirm the successful purification of small EVs from PC12 cells and demonstrate that α-synuclein is incorporated into secreted EVs. To assess whether α-syn-GFP is externally accessible or protected within intact EVs, α-syn-GFP-positive EVs were subjected to Proteinase K digestion, which has previously been shown to be a viable method to distinguish internal and external GFP markers in EVs[51,52]. No significant decrease in per-particle fluorescence or particle count was observed in the α-syn-GFP EV samples post Proteinase K treatment when single fluorescent EVs were visualised by wide-field fluorescence microscopy (Fig. 4G and Supp Info Video 1). Prior to digestion, α-syn-GFP EV preparations showed 17.8 ± 10.4 fluorescent EV particles over replicate 10 second video recordings, with an average maximum intensity of 272.6 arbitary units (a.u.) for identified EV particles. Following Proteinase K treatment, 39.3 ± 11.1 fluorescent EV particles were observed with a similar average maximum intensity of 277.7 a.u., indicating that a substantial fraction of the α-syn-GFP signal was resistant to proteolytic degradation. In contrast, the Control EV preparations showed very few detectable fluorescent particles, with 1.3 ± 1.9 pre–Proteinase K treatment, and 0 post Proteinase K treatmentThese data indicate that the observed fluorescent signal in the α-syn-GFP EV preparation is the result of internalised α-syn-GFP from donor cells.

Transferred α-syn exhibits nanoscale periodic organisation

The effect of exosomal α-syn contained in the conditioned medium requires dynamin-dependent uptake in recipient nerve terminals. To confirm that exosomal α-syn is indeed taken up by recipient neurons, we asked whether we could image it in recipient neurons. However, released exosomal α-syn is a relatively minor fraction of extracellular α-syn (Supp Fig. 2B). Further, the size of exosomes typically ranges from 30 to 100 nm, which is below the diffraction limit of light[53]. For these reasons, we turned to single molecule super-resolution microscopy to be able to detect sparse molecules of transmitted α-syn in recipient neurons. Recipient hippocampal neurons (DIV12-14) were incubated for 24 hours with conditioned medium from neurons expressing either mEos2 alone, α-syn^{WT}-mEos2, or α-syn^{A30P}-mEos2 (Fig. 5A). Neurons were pulsed for 5 minutes with CTB-Af647 in HK^{+} buffer and washed 3 times in LK^{+} buffer before a 2-hour incubation with the conditioned medium. We then performed single-particle tracking PhotoActivated Localization Microscopy (sptPALM) of either transmitted mEos2, α-syn^{WT}-mEos2 or α-syn^{A30P}-mEos2, which allows live tracking of individual molecules in living cells. As

expected, mEos2, α-syn^{WT}-mEos2 and α-syn^{A30P}-mEos2 were detected in the axons of recipient neurons that were positive for CTB-Af647 (Fig. 5B). Data analysis following tracking of individual trajectories was carried out and their nanoscale mobility was derived from the mean square displacement (MSD). The number of trajectories, their duration and the mobile/immobile ratio were also determined. Interestingly, the mobility of α-syn^{WT}-mEos2 was significantly reduced compared to that of mEos2 and α-syn^{A30P}-mEos2 (Fig. 4B) and displayed prominent periodicity (Fig. 5C). α-syn^{WT}-mEos2 molecules displayed a clustering behaviour with an average cluster size of 177 ± 5 nm, an average distance between clusters of 391 ± 23 nm and an average periodicity of 393 ± 26 nm. Notably, recipient neurons contained less transmitted α-syn^{WT}-mEos2 compared to mEos2 and the α-syn PD-linked mutant suggesting a potential effect of transmitted α-syn^{WT}-mEos2 on the uptake mechanism. However, the percentage of uptake was not significant between conditions (Fig. 5D). Furthermore, no significant difference was observed in trajectory duration nor in the mobile/immobile ratio (Fig. 5D).

Discussion

In this study, we show that α-syn^{WT}-containing EVs, but not α-syn^{A30P}, reduce axonal retrograde trafficking in recipient neurons. This effect depends on both Hsp90-mediated EV release from donor neurons and dynamin-dependent uptake in recipient neurons, linking α-syn-containing EVs secretion, cell-cell transfer and intracellular trafficking of signalling endosomes which are essential for neuronal survival[35,54]. These findings extend current models of disease with propagation of an α-syn mutant by showing that:

(1) EVs that contain either α-syn^{WT} or α-syn^{A30P} spread equally from cell to cell.

(2) α-syn^{WT}-containing EVs, reduce the retrograde flux of signalling endosomes in recipient neurons.

(3) α-sy^{A30P}-containing EVs, do not regulate retrograde trafficking, suggesting that the mutation leads to a loss of trafficking function in recipient neurons.

Synaptic dysfunction is increasingly recognised as an early event in Parkinson's disease (PD) and related synucleinopathies[55–58]. Consistent with this, α-syn accumulation at presynaptic terminals and axonal degeneration are prominent features of PD and dementia with Lewy bodies[59,60], and exogenous α-syn fibrils initiate pathology in axons before spreading to the soma[61]. Retrograde transport is essential for neuronal survival[2,62], and altered axonal transport protein expression have been reported in sporadic PD and experimental synucleinopathy models[56,63,64]. Our findings provide a mechanistic framework for these observations by showing that extracellular α-syn^{WT} selectively reduces retrograde trafficking in recipient neurons, suggesting that long-range axonal transport is normally controlled by transferred α-syn^{WT}.

Importantly, this regulation of neuronal trafficking is selective for α-syn^{WT} and is not observed with the α-syn^{A30P} disease-causing mutant, indicating that extracellular α-syn species differ in their ability to engage neuronal pathways in recipient cells. This distinction argues against a simple nonspecific toxic effect and instead supports a model in which α-syn^{WT} interacts with specific intracellular targets. In this context, the increased colocalisation of CTB with TrkB-positive compartments suggests that α-syn^{WT} regulates signalling endosome trafficking, potentially controlling neurotrophic signalling required for neuronal maintenance. This is consistent with previous work showing that exogenous α-syn fibrils can alter TrkB transport in hippocampal neurons[65].

The spatial orientation of this neuronal trafficking phenotype is interesting. Conditioned medium from α-syn^{WT}-expressing neurons reduces CTB retrograde transport only when applied to the nerve terminal compartment of microfluidic devices, not when applied to the soma. This suggests that α-syn acts locally at nerve terminals after entry into distal neuronal processes. Such a mechanism is consistent with *in vivo* studies in mice and non-human primates showing trans-synaptic propagation of α-syn[10,66] and supports the idea that early pathogenic events in synucleinopathies arise from local dysfunction at the presynapse.

Our results further establish EVs as functionally relevant carriers of α-syn. α-syn is released from neurons both as a free species[42,67–69] and in vesicle-associated forms[31,34,42,68,70]. Although exosomal α-syn represents only a minority of extracellular α-syn[71], our data indicate that this fraction is the biologically active population responsible for the observed trafficking phenotype. EVs purified from α-syn^{WT}-transfected donor cells exhibit the expected features of small EVs, including appropriate morphology, size distribution, enrichment of EV-associated markers, depletion of cellular contaminants, and they contain membrane-protected α-syn^{WT}-GFP cargo. The persistence of α-syn-GFP fluorescence after Proteinase K treatment supports the presence of protected intravesicular cargo and therefore a mode of transfer that is likely to preserve α-syn stability in the extracellular space. In line with previous reports that EV-associated α-syn can be internalised efficiently and exert stronger toxicity than exosome-free species[31,67], disruption of multivesicular body (MVB)-plasma membrane fusion abolished the neuronal retrograde trafficking of CTB, whereas immunodepletion of soluble α-syn did not rescue it. Together, these results indicate that EV-associated α-syn, although quantitatively minor, is functionally dominant in this system.

The EV-release experiments further support this interpretation. Using CD63-pHluorin, we found that exosome release from PC12 cells shows kinetics consistent with MVB fusion events[40,72,73] and is strongly reduced by expression of mutant Hsp90^{MD7}. Importantly, disrupting Hsp90 function abolished the effect of α-syn^{WT}-containing conditioned medium on retrograde trafficking, confirming that EV release is required for the phenotype. In hippocampal neurons, CD63-pHuji imaging indicated that α-syn-GFP is released in large vesicular packets, and that this release occurs similarly for α-syn^{WT}, α-syn^{A30P}

and EGFP, suggesting that the release step itself is generic, whereas the downstream functional consequences in recipient neurons are specific to α-syn^{WT}.

Our data indicate that internalisation of α-syn-containing EVs is dynamin-dependent. This is consistent with previous work showing endocytic uptake of α-syn fibrils and exosomal α-syn[9,42,74,75]. Although alternative uptake routes have been proposed in other cell types, differences in cellular context and the use of purified EVs versus conditioned medium likely explain these discrepancies[76]. In neurons, our findings support a model in which dynamin-dependent endocytosis is required for delivery of EV-associated α-syn cargo to intracellular compartments capable of dampening retrograde trafficking of signalling endosomes.

A particularly striking observation from our study is the periodic nanoscale organisation of transmitted α-syn^{WT} within recipient axons. Super-resolution imaging revealed that α-syn^{WT} exhibits lower mobility and a more structured distribution than α-syn^{A30P} or mEos2 alone, suggesting interaction with intracellular components that constrain its movement. This is consistent with the idea that α-syn^{WT} engages cytoplasmic or membrane-associated structures that may underlie its effect on trafficking. Previous studies have shown that exogenous α-syn can interact with endogenous α-syn[65,77–80], and our data raise the possibility that transmitted α-syn^{WT} is integrated into pre-existing neuronal architecture in a manner that promotes functional disruption. The periodicity of α-syn^{WT} clustering supports this interpretation and suggests that the pathological effect of α-syn may depend not only on its transfer, but also on its subcellular organisation after uptake.

Taken together, our findings support a model in which EV-mediated delivery of α-syn^{WT} to nerve terminals leads to local regulation of retrograde trafficking of neurotrophic signalling, resulting in early synaptic dysfunction. This provides a mechanistic framework linking α-syn propagation, transport defects and neuronal vulnerability in synucleinopathies. More broadly, our work suggests that extracellular α-syn should not be viewed solely as a transmissible aggregate, but as a biologically active cargo capable of altering intracellular trafficking pathways in recipient neurons. These findings nominate both EV-mediated transfer and endosomal trafficking pathways as candidate points for therapeutic intervention at early stages of disease progression.

Materials and Methods

Animal Research Ethics

All experiments using hippocampal neurons were performed on embryonic day 16 (E16) C57BL6/J mouse brains according to the guidelines of the Australian Code for the Care and Use of Animals for Scientific Purposes and were approved by the Animal Ethics Committee from the University of Queensland (QBI/254/16/NHMRC and QBI/244/19/NHMRC).

Reagents

The following reagents were sourced at Sigma-Aldrich: NaCl (746398), KCl (P3911), $MgCl_2$ (M9272), $CaCl_2$ (C5080), HEPES (H3375) ascorbic acid (A7506), Bovine serum albumin (BSA) (A8022). D-glucose was purchased from Amresco (0188). Anti-GFP magnetic beads were purchased from ChromoTek (GFP-Trap® Magnetic Agarose beads, gtma-20).

Hippocampal Neuronal Culture and Transfection

Murine hippocampal neurons were dissected from E16 C57BL6/J mice as previously described[81]. In brief, dissection of brains was performed in ice-cold dissection media (Milli-Q water, 1X Hank's balanced salt solution (14065-056, Gibco), 10 mM HEPES (15630080, Gibco), 100 units/mL-100 ug/mL Penicillin/Streptomycin (15140122, Gibco)). Trypsinisation of isolated hippocampi was performed by adding 30 µL of Trypsin (15090046, Gibco) followed by 10 minutes incubation at 37°C. Digestion was stopped by adding 150 µL of heat-inactivated horse serum (HS) (26050088, Gibco) and 50 µL of 1% DNAse I (D5025-375KU, Sigma-Aldrich) followed by another 10-minute incubation at 37°C. After trituration of the sample and centrifugation for 7 minutes at 15000 rpm, neurons from the pellet were resuspended in Plating medium (5% foetal bovine serum (FBS) (10099141, Gibco), 100 units/mL-100 ug/mL Penicillin/Streptomycin (15140122, Gibco), 1X GlutaMax™ (35050061, Gibco) in Neurobasal™ medium (21103-049, Gibco) and plated on either glass-bottom dishes (D29-20-1.5-N, Cellvis) or on custom microfluidic devices (see section "Microfluidic Devices Manufacturing") at a density of 80,000-100,000 for glass bottom dishes, and respectively 5,000 and 50,000 for the nerve terminal and soma chambers of microfluidic devices[81]. Prior to plating, dishes were coated with 1 mg/ml Poly-L-lysine (PLL) (P2636, Sigma-Aldrich) diluted in borate buffer (120 mM boric acid (B0394, Sigma-Aldrich)) and 70 mM di-sodium tetraborate decahydrate (SO0707, Scharlau) and incubated overnight at 37°C before being washed three times with ultra-pure distilled water (10977-015, Invitrogen). After 3–4 h, plating medium was replaced by Culture medium (1X B-27 Supplement (17504-044, Gibco), 1X GlutaMax™ (35050061, Gibco) and 100 units/mL Penicillin with 100 ug/mL Streptomycin (15140122, Gibco) in phenol-free Neurobasal™ medium (12348-017, Gibco)). Neurons were kept in the culture medium at 37°C with 5% CO_2 up to 20 days *in vitro* (DIV 20). 48 h prior to imaging, hippocampal neurons were transfected with plasmids (list provided in the section "Plasmids and Fluorescent Markers") using Lipofectamine™ 2000 (11668-019, Invitrogen) accordingly to the manufacturer's protocol.

Plasmids and Fluorescent Markers

EGFP-C1 and mCherry-N1 (632523) were purchased from Clontech and mEos2-N1 was purchased from Addgene (54662). α-syn^{WT}-GFP and α-syn^{A30P}-GFP (GFP on the N-terminus) were previously developed in the laboratory by Dr. Ye Jin Chai[82]. Hsp90^{WT}-mCherry and Hsp90^{MD7}-mCherry (mCherry on the C-terminus) were kindly provided by Dr. Patrik Verstreken (VIB-KU Leuven Center for Brain & Disease Research, Belgium). Hsp90^{MD7} has three mutations in its amphipathic helix: K392A, K395A and K399A. CD63-pHluorin and CD63-pHuji plasmids were kindly provided by Dr. Dirk Michiel Pegtel (Cancer Center Amsterdam, VU University Medical Center, Netherlands).

PC12 Cell Culture and Transfection

Rat pheochromocytoma cells (PC12) were cultured as previously described[83]. In brief, cells were grown in Culture medium (Dulbecco's Modified Eagle Medium supplemented with 7% heat-inactivated HS (26050088, Gibco), 7% heat-inactivated FBS (10099141, Gibco) and 0.85% GlutaMAX™ (35050061, Gibco)) at 37°C with 5% CO_2 in 75 mm^2 plastic culture flasks (156499, ThermoFisher). 24 h prior to transfection, cells were replated in 35 mm Nunc EasyDish™ plastic dishes (150460, ThermoFisher) or in 6-well plates (92006, TPP or 3516, Corning Costar). Transfection was carried out following the manufacturer's protocol using the Lipofectamine LTX™/Reagent Plus™ kit (15338-100, Invitrogen) mixed with plasmids (list provided in the section "Plasmids and Fluorescent Markers") in OPTIMEM™ (31985070, Gibco). After 24 h, conditioned medium was collected for immunodepletion and subsequent treatment of hippocampal neurons. Alternatively, the cells were replated in glass-bottom dishes (D29-20-1.5-N, Cellvis) for imaging. Before use, the dishes were coated overnight with 0.1 mg ml^{-1} poly-D-lysine (P0899, Sigma-Aldrich) prepared in 1× phosphate-buffered saline (PBS). The dishes were then washed three times with ultrapure distilled water (10977-015, Invitrogen).

Size-Exclusion Chromatography for Isolation of EVs

PC12 cells transfected with either EGFP-C1 or α-synWT–GFP were cultured in DMEM supplemented with 2.5% heat-inactivated, EV-depleted horse serum, 2.5% heat-inactivated, EV-depleted fetal bovine serum, and 1% GlutaMAX™. Conditioned medium was collected and used for extracellular vesicle isolation.

Approximately 100 mL of conditioned medium was concentrated to 1 mL using Amicon® Ultra-15 centrifugal filter units (UFC9010D, Merck). EVs were then isolated from the concentrated medium by size-exclusion chromatography using qEVoriginal columns (Generation 1, 70 nm; IC1-70, Izon) according to the manufacturer's instructions. To prepare EV-depleted serum, heat-inactivated serum was mixed with 0.22-µm-filtered 40% (w/v) polyethylene glycol 600 solution (PEG 600; 528877, Sigma-Aldrich), vortexed, and incubated for 1 h at 4°C. The samples were then centrifuged at 800 × g for 15 min, and the resulting supernatant was collected for use in cell culture medium.

Nanoparticle Tracking Analysis

EVs were measured via NanoSight Pro (Malvern Panalytical Ltd, Malvern), equipped with a 642 nm laser. Automatic camera, focus and number of frame settings were used, with a flow rate of 1.5 µL/min.

Cryo-TEM

Cryo-TEM was used to identify phospholipid bilayers, a key authentication feature of EVs. EV samples were prepared for imaging using a Leica EM GP2 robotic vitrification system (Leica, Germany), under controlled temperature (22°C) and humidity (95%). Samples (3 µL) were dispersed onto a Lacey formvar carbon-Cu, 200 mesh grid (Electron Microscopy Services). Excess solution was mechanically blotted away for 2.5–3.5 s. Subsequently, samples were mechanically plunged into − 182.8°C liquid ethane, to vitrify the sample. Samples were stored in liquid nitrogen prior to imaging using a Jeol Cryo ARM 300 (JEM-Z300FSC) TEM equipped with a cold field emission gun and an Omega energy filter. Images were captured at a 300 kV acceleration voltage and 20 eV filter setting, with zero energy loss. Images were

acquired under low-dose conditions by a Gatan K3 direct detector camera and processed using the Serial EM software.

Western Blot

Sample protein concentrations were determined using the Pierce Micro BCA Protein Assay Kit (Thermo Fisher Scientific, 23235). Samples were diluted in sucrose buffer and mixed with 4× Laemmli Sample Buffer (Bio-Rad, 1610747) before heating at 90°C for 5 min. Equal amounts of protein (1.22 µg/well), were loaded per well alongside Precision Plus Protein Kaleidoscope Prestained Protein Standards (Bio-Rad, 1610375), onto NuPAGE 4–12% Bis-Tris protein gels, 1.5 mm (Invitrogen, NP0321). Gels were run in 1× NuPAGE MOPS SDS Running Buffer (Invitrogen, NP0001). Electrophoretic separation was performed at 200 V for 45 min. Following electrophoresis, proteins were transferred in 1× Tris-glycine transfer buffer. Transfer was performed at 100 V for 1.5 h. Membranes were blocked for 1 h at room temperature in 5% skim milk in TBST with gentle agitation. Membranes were incubated overnight at 4°C with primary antibodies diluted in 1% skim milk in TBST. The following primary antibodies were used: ALIX (1:200, Cell Signaling Technology, 2171S), calnexin (1:250, GeneTex, GTX112886), and CD81 (1:500, Santa Cruz Biotechnology, sc-166029). After primary antibody incubation, membranes were washed four times for 5 min each in 1× TBST. Membranes were then incubated for 1 h at room temperature, protected from light, with near-infrared fluorescent secondary antibodies diluted in 1% skim milk in TBST. The secondary antibodies used were IRDye 680-conjugated anti-mouse IgG and IRDye 800-conjugated anti-rabbit IgG at 1:2000 dilution. Following secondary antibody incubation, membranes were washed three times for 5 min each in 1× TBST, followed by a final rinse in TBS. Membranes were imaged using the 700 nm and 800 nm fluorescence channels on a ChemiDoc MP Imaging System (Bio-Rad), and images were acquired under non-saturating conditions.

Characterization of luminal cargo of α syn EVs

Proteinase-k digestion of unprotected GFP was performed using a modified protocol from Cvjetkovic et al., 2016. Briefly, to normalise protein concentrations for proteinase-k digestion, the total protein concentration of α-syn-GFP EVs was determined using the Micro BCA™ Protein Assay Kit (Thermo Fisher Scientific). EVs were lysed with a 4% (w/v) SDS solution mixed 1:1 with the EV suspension. Samples were incubated on ice for 30 min to promote vesicle lysis and release of protein cargo. The lysed samples were subsequently diluted 10-fold in Milli-Q water prior to protein quantification. Protein concentrations were calculated from a bovine serum albumin standard curve prepared according to the manufacturer's protocol. 100ug/ml of α-syn-GFP EVs were then incubated with 20 µg/mL Proteinase K (Qiagen) in PBS for 2 h at 37°C with shaking at 300 rpm using a thermomixer. Proteinase K digestion activity was verified using free GFP following the same digestion protocol, with bulk fluorescence measured by plate reader (Tecan Infinite M Plex). 100 µL working solution of EV samples pre and post proteinase K digestion were loaded into a glass-bottom 96-well plate (Corning #4580) and wide-field fluorescent microscopy was performed using a Nikon TE2000 microscope, configured with a Plan Apo VC 60×/1.40 oil DIC N2 objective, X-Cite Series 120 Q illumination source, FITC-compatible filter set (Chroma Technology Corp) and Primer BSI Express sCMOS camera. Fluorescent microscopy of single

EVs were obtained as videos, recorded with 50x50 µm ROIs, 50ms exposure, for 10 seconds. At least 3n replicates were recorded for each sample. Fluorescent EV videos were processed by using FIJI (Image J 1.54p) with Trackmate software[84]. Videos were calibrated for spatial scale and frame rate, and the full field of view was selected as the region of interest. Particles were detected using the LoG detector, with parameters optimised on representative frames to ensure accurate identification of fluorescent EVs. Detected particles were linked using the Simple LAP tracker, and only tracks persisting for approximately five frames or longer were retained to minimise transient background detections. The total number of valid tracks was used as the fluorescent EV particle count, while maximum fluorescence intensity per track was used to calculate the mean maximum intensity and standard deviation for each replicate. Erroneous zero-valued tracks were excluded from analysis.

Mass Spectrometry Sample Processing

Sample processing of whole cell lysates and purified exosome fractions was performed as follows. Samples were resuspended in lysis buffer consisting of 2% v/v sodium dodecyl sulfate, 50% v/v trifluoroethanol, and 10 mM phosphate buffer, pH 7.4, containing 10 mM dithiothreitol. Protein denaturation and disulfide bond reduction were performed by heating to 60°C for 30 min in a heating block. Cysteine residues were then alkylated to prevent disulfide bond reformation using 50 mM iodoacetamide for 45 min at RT in the dark. Proteins were then precipitated through the addition of 10 volumes of ice-cold 1:1 methanol/isopropanol, followed by overnight incubation at − 20°C. Precipitates were pelleted by centrifugation at 14,000 g for 60 min in a benchtop microfuge. The supernatant was removed, and the pellet was washed with the addition of 1 mL of ice-cold 1:1 methanol/isopropanol, followed by a second round of centrifugation as previously described. The pellet was resuspended in 100 µL of 50 mM ammonium bicarbonate containing 2 µg of proteomics-grade trypsin (Sigma-Aldrich). Proteolytic digestion was performed overnight at 37°C in a shaking incubator set to 250 rotations/min. Peptides were desalted using a SolaU reverse-phase solid-phase extraction cartridge, evaporated to dryness, and stored at − 20°C. Prior to analysis, samples were resuspended in 20 µL of 0.1% trifluoroacetic acid, and the purified peptide concentration was quantified using a micro bicinchoninic acid total protein kit (Pierce). All sample concentrations were normalised to 1 µg of peptide extract per 4 µL.

Untargeted Mass Spectrometry

Unknown protein identification was performed by injecting 1 µg of peptide digest onto a 7600 ZenoTOF mass spectrometer (AB Sciex) coupled to an M-Class Acquity LC (Waters). Chromatographic conditions consisted of first injecting the sample onto a 0.3 × 10 mm C18 micro-trapping column (Phenomenex) under an isocratic flow of 0.1% formic acid at 10 µL/min. After 10 min, the trapping column was switched in-line with the separation column (BIOshell™ 0.3 × 150 mm C18 with 2.7 µm particle size, Supelco). Gradient mobile phases consisted of A) 0.1% formic acid and B) acetonitrile containing 0.1% formic acid, at a flow rate of 5 µL/min. Chromatographic separations started at 5% B, progressing to 35% B at 38 min, 80% B at 39 min, plateauing until 43 min, before dropping to 5% B at 80 min, followed by aqueous column re-equilibration for 2 min. MS analyses were performed using positive mode

electrospray ionisation (ESI) with variable window data-independent data acquisition. Source conditions consisted of curtain, GS1, and GS2 gases set to 30, 30, and 20 psi, respectively; source temperature at 250°C; and ion spray and declustering potentials set to 5500 V and 100 V, respectively. Protein identification and quantification were performed using the DIA-NN software platform (Demichev, 2020), screening against the mouse proteome obtained from the UniProt database using a 1% false discovery rate threshold for peptide-level identification. Data analysis was performed in Excel and GraphPad Prism.

Targeted Analysis of α-synuclein

A bespoke targeted multiple reaction monitoring (MRM) LC-MS/MS assay was employed for quantification of *Homo sapiens* α-synuclein (P37840), targeting tryptic peptides (Table 1) determined using the Skyline software platform (MacCoss Laboratory) and validated to be proteotypic for α-synuclein by BLAST search against the mouse proteome using the UniProt online resource.

Table 1
Target peptides for comparative quantification of α-synuclein

Peptide	**Ion**	**Precursor *m/z***	**Collison Energy (CE)**	**Quantification Fragment**
EGVLYVGSK	M+2H	437.2374	22.3	y5
EQVTNVGGAVVTGVTAVAQK	M+3H	643.3530	28.9	y8
TVEGAGSIAAATGFVK	M+2H	739.8961	35.3	y8

Liquid chromatography–mass spectrometry was performed using 1 µg of peptide digest analysed on a 7600 ZenoTOF mass spectrometer (AB Sciex) coupled to an M-Class Acquity LC (Waters), using the same chromatographic conditions as described for untargeted proteomics. Mass spectrometry analysis was performed using a positive-mode ESI source under conditions as described for untargeted proteomics analysis. Data acquisition was performed using product ion scans targeting the ions described in Table 1, using a 100 ms accumulation time per ion. Data analysis was performed using the Skyline software package. Chromatographic peaks corresponding to target peptides were identified by matching MS/MS fragmentation spectra with predicted fragmentation based on amino acid composition. Peptide intensity was quantified using the peak area of the highest responding fragment ion (Table 1). Statistical analysis and data visualisation were performed in GraphPad Prism.

Microfluidic Device Manufacture

Microfluidic devices were custom-made to fit inside a glass-bottom dish (D29-20-1.5-N, Cellvis) as previously described[81]. Microfluidic devices allow separation of axons from cell bodies to facilitate the study of axonal transport[85]. Upon receipt, devices were rinsed one time with UltraPure™ DNase/RNase-Free Distilled Water (10977-015, Invitrogen) followed by a coating step with PLL and seeding of hippocampal neurons in the devices[81].

Neuronal Treatment, Stimulation, and Nerve Terminal Labelling with CTB

On DIV 11–13, the hippocampal neurons seeded in the soma chamber of the microfluidic devices were transfected using Lipofectamine™ 2000 (11668-019, Invitrogen) accordingly to the manufacturer's protocol. Used plasmids are listed in the section "Plasmids and Fluorescent Markers". After 24 h, the conditioned medium from the soma chamber was harvested and mixed in a ratio of 70/30 (v/v) with the conditioned medium from the nerve terminal chamber of another microfluidic device seeded with naïve hippocampal neurons. This mix of media was consequently applied either to the soma chamber or nerve terminal chamber of the device containing naïve hippocampal neurons. On DIV 13–15, treated microfluidic devices were stimulated with a "pulse" corresponding to addition of high potassium (HK^+) buffer (56 mM KCl, 0.5 mM ascorbic acid, 0.1% BSA, 15 mM HEPES, 5.6 mM D-Glucose, 95 mM NaCl, 0.5 mM $MgCl_2$, 2.2 mM $CaCl_2$, pH 7.4 and osmolarity 290–310) to the soma chamber, and addition of HK^+ buffer containing Cholera toxin subunit B conjugated to either Alexa Fluor™ 555 or Alexa Fluor™ 647 (CTB-Af555 or CTB-Af647) (50 ng/ml) (C34776 and C34778 respectively, Invitrogen) to the nerve terminal chamber of the microfluidic device. The device was then incubated 5 minutes at 37°C before a washing step consisting of three washes with low potassium (LK^+) buffer (5.6 mM KCl, 0.5 mM ascorbic acid, 0.1% BSA, 15 mM HEPES, 5.6 mM D-Glucose, 145 mM NaCl, 0.5 mM $MgCl_2$, 2.2 mM $CaCl_2$, pH 7.4 and osmolarity 290–310) to remove excess of CTB that has not been endocytosed. Finally, the LK^+ buffer was replaced by the original conditioned medium and the device was put back at 37°C for a 2 h chase. After the chase, live imaging of CTB-Af555 or CTB-Af647 undergoing retrograde transport in axons crossing the grooves of the microfluidic device was performed using a microscope equipped with an incubation system that enables imaging at 37°C and 5% CO_2 (Diskovery spinning disk confocal microscope or a Zeiss Elyra SIM/PALM/STORM super-resolution microscope).

Depletion of α-syn from Conditioned Medium

PC12 cells were co-transfected with either α-syn^{WT}-GFP and Hsp90^{WT}-mCherry or α-syn^{WT}-GFP and Hsp90^{MD7}-mCherry for 24 h. Following transfection, conditioned medium from cells expressing α-syn^{WT}-GFP and Hsp90^{WT}-mCherry was collected and immunodepleting was conducted using GFP-Trap® Magnetic Agarose beads (ChromoTek) according to manufacturer's protocol. Briefly, beads were incubated with the conditioned medium (25 µL of beads for 1 mL of medium) for 1 hour at 4°C under rotation. Magnetic beads were then separated by placing tubes containing the conditioned medium on a magnetic rack and removing the supernatant. Afterwards, the supernatant depleted of free α-syn was incubated with naïve neurons seeded in microfluidic devices to analyse the effect of the depleted medium on retrograde transport of CTB in the recipient neurons (see section "Neuronal Treatment, Stimulation, and Nerve Terminal Labelling with CTB" for detailed protocol). Imaging was performed on a Diskovery spinning disk (see section "Diskovery Spinning Disk Confocal Imaging and Analysis" for details). Immunodepleted conditioned medium was assessed for α-syn by running on SDS-PAGE gel and

Western-blotting. In brief, conditioned medium samples were solubilised in either 2X sodium dodecyl sulfate (SDS) with 10% β-mercaptoethanol (for the original medium) or in 1X SDS with 10% β-mercaptoethanol (for the depleted medium) and boiled at 95°C for 5 minutes. Equal amounts of proteins were then loaded on a Tris-Glycine precast gel (4–15%, Bio-Rad), ran at 100 V for an hour and subsequently transferred onto an Immobilon®-FL PVDF membrane (05317, Millipore) and incubated for 1 h in blocking buffer (Odyssey® Tris-Buffered Saline, Li-Cor). Afterwards, membranes were incubated in a mix of 1X PBS/0.2% Tween® 20 (P1379, Sigma-Aldrich) with primary antibodies overnight at 4°C (mouse anti-α-syn, 1:250, Abcam ab27766 and rabbit anti-GFP, 1:1000, Millipore AB3080P). Membranes were then washed 3 times for 10 minutes with Tris-Buffered Saline/0.2% Tween® 20 (P1379, Sigma-Aldrich) and incubated in blocking buffer (Odyssey® Tris-Buffered Saline, Li-Cor) containing InfraRed secondary antibody diluted 1:20,000 (goat anti-rabbit IRDye® 680LT, 926-68021 and goat anti-mouse IRDye® 800CW, 926-32210, Millennium Sciences).

Diskovery Spinning Disk Confocal Imaging and Analysis

Time-lapse imaging was performed at the Queensland Brain Institute's Advanced Microscopy Facility using a Nikon Plan CFI Apo Lambda 60x Oil objective (Numerical Aperture 1.45, W.D. 0.13 mm) on a spinning disk confocal microscope (Diskovery; Andor Technology, UK), equipped with 4 laser lines (405 nm, 588 nm, 561 nm and 640 nm), 500 µm wide range piezo z-drive, two Zyla 4.2 sCMOS cameras (Andor Technology), and built around a Nikon Ti-E body (Nikon Corporation, Japan) and controlled by Nikon NIS software (version 5.2). Live movies were acquired at 3.3 Hz with 300 ms exposure using the 100 nm pinhole. Movies were then deconvoluted using Huygens (version 17.10–64 and 18.04-64) and analysed using ImageJ (version 1.53) with the TrackMate plugin (version 3.4.2) to track the number of CTB+ carriers. The data generated by TrackMate were then processed using R (version 1.2.1335) to obtain final data on the frequency of CTB+ carriers. Kymographs were generated using the KymographBuilder plugin (version 2.1.1) on ImageJ.

Exosomal release live imaging and analysis

48 h after transfection, PC12 cells or hippocampal neurons (DIV 18) cultured in glass-bottom dishes were washed once with imaging buffer (145 mM NaCl, 5 mM KCl, 1.2 mM Na_2HPO_4, 20 mM HEPES and 10 mM D-glucose, pH 7.4) or LK+ buffer (5.6 mM KCl, 0.5 mM ascorbic acid, 0.1% BSA, 15 mM HEPES, 5.6 mM D-Glucose, 145 mM NaCl, 0.5 mM $MgCl_2$, 2.2 mM $CaCl_2$, pH 7.4 and osmolarity 290–310) for PC12 cells or neurons respectively, before imaging at the Queensland Brain Institute's Advanced Microscopy Facility using the Roper iLas 2 microscope (generously supported by the Australian Government through the ARC LIEF grant LE130100078). For experiments characterising the effect of $Hsp90^{MD7}$ on exosomal release in PC12 cells, prior to each time-lapse recording, $Hsp90^{MD7}$expression level in the cell was verified by acquiring an image in the red (561) channel. Analysis of exosomal release was performed using ImageJ (version 1.53). Where needed, raw movies were drift corrected using the Stabilizer plugin. Exosomal release in PC12 cells transfected with CD63-pHluorin was characterised by a burst in fluorescence in the green (488) channel, corresponding to the fusion of MVBs with the plasma

membrane leading to neutralisation of the pH in the MVB lumen and unquenching of fluorescence. One burst of fluorescence was called a “fusion event”. For each recording, the number of fusion events and the duration of each event were determined. The duration of an event was defined from the time point fluorescence started to increase until the fluorescence had returned to the basal level. When there was no return to initial fluorescence, the end time point was determined as the time when the fluorescence reached a steady state. Regarding exosomal release of α-syn in hippocampal neurons, analysis of exocytic events was performed with the Bar plugin of ImageJ, which provided measurements of fluorescence over time in both red and green channels in hippocampal neurons transfected with CD63-pHuji and α-syn-GFP. A “fusion event” was defined by a sharp decrease in fluorescence in the red channel. For each recording, the number of fusion events and their dynamics (event duration, rise time, decay time, maximum fluorescence, amplitude of fluorescence variation) were determined. The duration of an event was defined in the red channel from the time point fluorescence started to decrease until the moment fluorescence had reached a plateau. In the green channel, an event was defined from the time point fluorescence started to increase until the time fluorescence had returned to the basal level or reached steady state if there was no decrease.

TIRF Microscopy - Roper iLas 2 Microscope

Time-lapse total internal reflection fluorescence (TIRF) imaging was performed on a motorized inverted microscope (Nikon, TiE) equipped with a perfect focus system with an iLas2 double-laser illuminator (Roper Scientific), two Evolve 512 delta EMCCD cameras (Photometrics) mounted on a TwinCam LS Image Splitter (Cairn Research) and an incubation system. The microscope has 2 sets of optical filters, one being within the microscope’s body: a QUAD dichroic filter (ZT405/488/561/647rpc, Chroma) with a QUAD emission filter (ZET405/488/561/640m, Chroma), the second set being within the splitter. The splitter contains a dichroic filter and two emissions filters which can be changed depending on the experimental design. The classic setting comprises the dichroic ZT647rdc-UF1 (Chroma) and two emission filters (Chroma): ET690/50m and ZET405/488/561m. For dual live imaging of α-syn-GFP and CD63-pHuji, the dichroic filter and emission filters on the splitter were changed for: the dichroic filter T565lpxr (Chroma), emission filters ET600/50m and ET540/40m (Chroma). Prior to imaging, alignment of cameras and TIRF angle calibration were performed using TetraSpeck™ microspheres beads (T729, Invitrogen). Neurons were maintained at 37°C and 5% CO_2 during imaging. Time-lapse movies were acquired using a TIRF angle allowing selective imaging of the plasma membrane. Laser power was set at 6.5% for the 561 channel and 10.5% for the 488 channel and recording was performed at 2 Hz with 20 ms exposure over 10 minutes. Stimulation was performed at 5 minutes by adding either 2 mM barium chloride (100474N, BDH Reagents & Chemicals) to PC12 cells, or HK+ buffer (56 mM KCl, 0.5 mM ascorbic acid, 0.1% BSA, 15 mM HEPES, 5.6 mM D-Glucose, 95 mM NaCl, 0.5 mM $MgCl_2$, 2.2 mM $CaCl_2$, pH 7.4 and osmolarity 290–310) to hippocampal neurons. Image acquisition was performed using MetaMorph® (version 7.10.1.161; Molecular Devices).

Single-Particle Tracking Photoactivated Localization Microscopy (sptPALM)

A day after transfecting hippocampal neurons (DIV 11–13) of the soma chamber of microfluidic devices with either mEos2 alone, α-syn^{WT} -mEos2 or α-syn^{A30P}-mEos2, conditioned media from the soma chambers was collected and mixed with conditioned media from the nerve terminal chamber of naïve recipient neurons (70/30 vol/vol ratio) before adding the mix to recipient neurons of the nerve terminal chamber (DIV 12–14) for 24 hours. After a 5-minute pulse and 2 h chase, time-lapse imaging was performed at the Queensland Brain Institute's Advanced Microscopy Facility using an Alpha Plan-Apochromat 100X (1.46 NA) oil objective on the Zeiss ELYRA SIM/PALM/STORM microscope equipped with an Andor 897 EMCCD camera and an incubation system allowing imaging under 37°C and 5% CO_2 conditions. Time-lapse movies were acquired using a total internal reflection fluorescence (TIRF) angle allowing selective imaging of the plasma membrane. Axons were located using the 642 nm laser to visualise CTB-Af647 taken up by neurons. Imaging of CTB was performed with 1% laser power and a 300 ms exposure time over 400 frames. Subsequently, imaging of transmitted mEos2 molecules within neurons was achieved using the 405 nm and 561 nm lasers to respectively photoconvert and visualise mEos2 molecules. The 405 nm laser was used at 2-.3% power, whereas the 561 nm laser was used at 30% power. Acquisition was performed over 2000 or 16000 frames and 30 ms exposure time using the Zen acquisition software (Black edition, 2012 version, Carl Zeiss).

sptPALM Analysis and Cluster Analysis

ImageJ (version 1.53) was used to convert movies from Zen's CZI format to a TIFF format. The localisation and mobility of single molecules was determined using aPALMtracer plugin in MetaMorph. The analysis was done for specific regions of interest (ROIs) as well as for the whole field of view. ROIs were drawn around axons based on the maximum Z projection image of CTB-Af647 molecules moving within axonal projections situated in the nerve terminal chamber of microfluidic devices. PALMTracer generated trajectory maps, super-resolved average intensity, and diffusion coefficient (D) maps as well as excel files containing diffusion coefficient and mean square displacement (MSD) values. Thresholding of the signal was done individually for each movie. Only molecules that were picked up by the thresholding and whose fluorescence lasted across at least eight frames of the movie were tracked. The mean square displacement was determined for each trajectory using the equation $MSD\ (t) = a + 4Dt$ where "a" is the offset constant which incorporates the effects of localization error and finite camera exposure, "D" is the diffusion coefficient and "t" is the time. The first eight points of the MSD were averaged for all trajectories and plotted against time. The area under the MSD curve (AUC) was used to quantify the significance of change in MSD values. Molecules were distributed into mobile and immobile populations based on the value of the diffusion coefficient where log10(D) > -1.5 $\mu m^2 s^{-1}$ was considered the mobile fraction [81]. The percentage of molecules that were taken up by neurons was determined using the following formula: ((Number of tracks. μm^{-1} in neurons) - (Number of tracks. μm^{-1} without ROI) / (Number of tracks. μm^{-1} in neurons)) * 100. The periodicity analysis of clusters was done on the intensity average map produced by PalmTracer using ImageJ where a line was drawn between each cluster to determine the spacing between clusters, and from one edge of a cluster

to the other edge to determine the cluster size. Additional cluster analysis was performed by using the Nanoscale Spatiotemporal Indexing Clustering (NASTIC) tool on data output by PALMTracer, as previously described[86].

Statistical analysis

GraphPad Prism 9.4.1 (San Diego, USA) was used to determine statistical significance and determine outliers using the ROUT method. Normal distribution of data was tested using the "D'Agostino-Pearson omnibus" normality test. For comparison between two groups that were normally distributed, a Student's t test was used. For unpaired non-parametric data sets, a Mann-Whitney test was used, and for paired data sets a Wilcoxon signed-rank test was used. For datasets which compared more than 2 groups, an ANOVA was used with multiple comparisons (for normally distributed data, an ordinary one-way ANOVA with Tukey's multiple comparisons was performed; for non-parametric data, Kruskal-Wallis test with Dunn's multiple comparisons was performed). Tests used are indicated in the respective figure legends. p values < 0.05 were considered statistically significant.

Declarations

Data Availability

All processed data will be made available upon request and stored on The University of Queensland data repository, UQ eSpace.

Conflict of Interest

The authors have no conflict of interest to declare.

Authors' contributions

All authors contributed to the study by performing experiments, performing data analysis, providing interpretation, supplying reagents or writing the manuscript. F.A.M. conceived the study and B.E.D. and V.L. coordinated and performed the study. B.E.D. prepared the figures and wrote the manuscript with F.A.M., R.S.G., T.P.W. and A.J.M., with editing and input from co-authors. V.L. performed the immunohistochemistry, the immunodepletion of the conditioned medium, Western Blots, all CTB retrograde transport experiments and their analyses. B.E.D. performed Hsp90 characterisation experiments, the exosomal release experiments as well as the super resolution experiments and their analyses. A.T.B. provided technical support for the super-resolution experiments. R.S.G., T.P.W. and A.J.M. gave input on figures and participated in manuscript writing. J.J.C-W. provided the microfluidic devices. P.V. provided the Hsp90 constructs.

Acknowledgments

The authors acknowledge the use of the Australian Microscopy & Microanalysis Research Facility at The University of Queensland. We thank IT department and the Advanced Microscopy and Microanalysis Facility at the Queensland Brain Institute for their outstanding support. We thank Dr. Dirk Michiel Pegtel for providing the CD63 constructs. The work was supported by an Australian Research Council (ARC) Discovery Project grant (DP170100125), an ARC Linkage Infrastructure Equipment and Facilities grant (LE130100078) and a National Health and Medical Research Council (NHMRC) Senior Research Fellowship (1155794) to F.A.M. The Research Training Program (RTP) Scholarship and a QBI top-up Scholarship supported work conducted by B.E.D.

References

1. Wang T et al (2015) Control of autophagosome axonal retrograde flux by presynaptic activity unveiled using botulinum neurotoxin type a. J Neurosci 35:6179–6194
2. Wang T et al (2016) Flux of signalling endosomes undergoing axonal retrograde transport is encoded by presynaptic activity and TrkB. Nat Commun 7:12976
3. Maday S, Holzbaur EL (2012) Autophagosome assembly and cargo capture in the distal axon. Autophagy 8:858–860
4. Ye H, Kuruvilla R, Zweifel LS, Ginty DD (2003) Evidence in support of signaling endosome-based retrograde survival of sympathetic neurons. Neuron 39:57–68
5. Braak H et al (2003) Staging of brain pathology related to sporadic Parkinson’s disease. Neurobiol Aging 24:197–211
6. Spillantini MG, Crowther RA, Jakes R, Hasegawa M, Goedert M (1998) α-Synuclein in filamentous inclusions of Lewy bodies from Parkinson’s disease and dementia with Lewy bodies. *Proceedings of the National Academy of Sciences* 95, 6469–6473
7. Spillantini MG (1999) Parkinson's disease, dementia with Lewy bodies and multiple system atrophy are α-synucleinopathies. Parkinsonism Relat Disord 5:157–162
8. Li J-Y et al (2008) Lewy bodies in grafted neurons in subjects with Parkinson's disease suggest host-to-graft disease propagation. Nat Med 14:501–503
9. Hansen C, Li J-Y (2012) Beyond α-synuclein transfer: pathology propagation in Parkinson's disease. Trends Mol Med 18:248–255
10. Luk KC et al (2012) Pathological α-synuclein transmission initiates Parkinson-like neurodegeneration in nontransgenic mice. Science 338:949–953
11. Angot E et al (2012) Alpha-synuclein cell-to-cell transfer and seeding in grafted dopaminergic neurons in vivo. PLoS ONE 7:e39465
12. Masuda-Suzukake M et al (2013) Prion-like spreading of pathological α-synuclein in brain. Brain 136:1128–1138
13. Peelaerts W et al (2015) α-Synuclein strains cause distinct synucleinopathies after local and systemic administration. Nature 522:340–344

14. Watts JC et al (2013) Transmission of multiple system atrophy prions to transgenic mice. *Proceedings of the National Academy of Sciences* 110, 19555–19560
15. Prusiner SB et al (2015) Evidence for α-synuclein prions causing multiple system atrophy in humans with parkinsonism. *Proceedings of the National Academy of Sciences* 112, E5308–E5317
16. Ayers JI et al (2022) Different α-synuclein prion strains cause dementia with Lewy bodies and multiple system atrophy. *Proceedings of the National Academy of Sciences* 119, e2113489119
17. Kinet R et al (2025) Differential pathological dynamics triggered by distinct Parkinson patient–derived α-synuclein extracts in nonhuman primates. Sci Adv 11:eadu6050
18. Maroteaux L, Campanelli JT, Scheller RH (1988) Synuclein: a neuron-specific protein localized to the nucleus and presynaptic nerve terminal. J Neurosci 8:2804–2815
19. Iwai A et al (1995) The precursor protein of non-Aβ component of Alzheimer's disease amyloid is a presynaptic protein of the central nervous system. Neuron 14:467–475
20. Yang M-L, Hasadsri L, Woods WS, George JM (2010) Dynamic transport and localization of alpha-synuclein in primary hippocampal neurons. Mol neurodegeneration 5:9
21. Del Mar C, Greenbaum EA, Mayne L, Englander SW, Woods VL Jr (2005) Structure and properties of α-synuclein and other amyloids determined at the amino acid level. *Proceedings of the National Academy of Sciences* 102, 15477–15482
22. Fauvet B et al (2012) Characterization of semisynthetic and naturally Nα-acetylated α-synuclein in vitro and in intact cells: implications for aggregation and cellular properties of α-synuclein. J Biol Chem 287:28243–28262
23. Burré J, Sharma M, Südhof TC (2014) α-Synuclein assembles into higher-order multimers upon membrane binding to promote SNARE complex formation. *Proceedings of the National Academy of Sciences* 111, E4274–E4283
24. Wang L et al (2014) α-synuclein multimers cluster synaptic vesicles and attenuate recycling. Curr Biol 24:2319–2326
25. Vasili E, Dominguez-Meijide A, Outeiro T (2020) Spreading of a-Synuclein and Tau: A Systematic Comparison of the Mechanisms Involved. Protein Misfolding Spreading Pathol Neurodegenerative Dis 10:10743
26. Valdinocci D, Radford RA, Siow SM, Chung RS, Pountney DL (2017) Potential modes of intercellular α-synuclein transmission. Int J Mol Sci 18:469
27. Bobrie A, Colombo M, Raposo G, Théry C (2011) Exosome secretion: molecular mechanisms and roles in immune responses. Traffic 12:1659–1668
28. Gurung S, Perocheau D, Touramanidou L, Baruteau J (2021) The exosome journey: from biogenesis to uptake and intracellular signalling. Cell Communication Signal 19:47
29. Théry C (2011) Exosomes: secreted vesicles and intercellular communications. F1000 biology Rep 3:15

30. Hamamichi S (2009) Identification of neuroprotective genes against alpha-synuclein toxicity using a Caenorhabditis elegans Parkinson disease model. The University of Alabama
31. Danzer KM et al (2012) Exosomal cell-to-cell transmission of alpha synuclein oligomers. Mol neurodegeneration 7:42
32. Shi M et al (2014) Plasma exosomal α-synuclein is likely CNS-derived and increased in Parkinson's disease. Acta Neuropathol 128:639–650
33. Sepúlveda D, Cisternas-Olmedo M, Arcos J, Nassif M, Vidal RL (2022) Contribution of autophagy-lysosomal pathway in the exosomal secretion of alpha-synuclein and its impact in the progression of Parkinson's disease. Front Mol Neurosci 15:805087
34. Jiang C et al (2020) Serum neuronal exosomes predict and differentiate Parkinson's disease from atypical parkinsonism. J Neurol Neurosurg Psychiatry 91:720–729
35. Lauwers E et al (2018) Hsp90 mediates membrane deformation and exosome release. Mol Cell 71:689–702
36. Bruyere J et al (2020) Presynaptic APP levels and synaptic homeostasis are regulated by Akt phosphorylation of huntingtin. *elife* 9, e56371
37. Fussi N et al (2018) Exosomal secretion of α-synuclein as protective mechanism after upstream blockage of macroautophagy. Cell Death Dis 9:757
38. Wardhani K, Levina A, Grau GE, Lay PA (2024) Fluorescent, phosphorescent, magnetic resonance contrast and radioactive tracer labelling of extracellular vesicles. Chem Soc Rev 53:6779–6829
39. Verweij FJ et al (2018) Quantifying exosome secretion from single cells reveals a modulatory role for GPCR signaling. J Cell Biol 217:1129–1142
40. Bebelman MP et al (2020) Real-time imaging of multivesicular body–plasma membrane fusion to quantify exosome release from single cells. Nat Protoc 15:102–121
41. Gustafsson G et al (2018) Secretion and uptake of α-synuclein via extracellular vesicles in cultured cells. Cell Mol Neurobiol 38:1539–1550
42. Lee H-J, Patel S, Lee S-J (2005) Intravesicular localization and exocytosis of α-synuclein and its aggregates. J Neurosci 25:6016–6024
43. Grozdanov V, Danzer KM (2018) Release and uptake of pathologic alpha-synuclein. Cell Tissue Res 373:175–182
44. Stefanis L et al (2019) How is alpha-synuclein cleared from the cell? J Neurochem 150:577–590
45. Christensen DP, Ejlerskov P, Rasmussen I, Vilhardt F (2016) Reciprocal signals between microglia and neurons regulate α-synuclein secretion by exophagy through a neuronal cJUN-N-terminal kinase-signaling axis. J Neuroinflamm 13:59
46. Sung JY et al (2001) Induction of neuronal cell death by Rab5A-dependent endocytosis of α-synuclein. J Biol Chem 276:27441–27448
47. Alvarez-Erviti L et al (2011) Lysosomal dysfunction increases exosome-mediated alpha-synuclein release and transmission. Neurobiol Dis 42:360–367

48. Wu Y et al (2014) A dynamin 1-, dynamin 3-and clathrin-independent pathway of synaptic vesicle recycling mediated by bulk endocytosis. Elife 3:e01621
49. Gormal R, Valmas N, Fath T, Meunier F (2017) A role for tropomyosins in activity-dependent bulk endocytosis? Mol Cell Neurosci 84:112–118
50. Harper CB, Popoff MR, McCluskey A, Robinson PJ, Meunier FA (2013) Targeting membrane trafficking in infection prophylaxis: dynamin inhibitors. Trends Cell Biol 23:90–101
51. Cvjetkovic A et al (2016) Detailed Analysis of Protein Topology of Extracellular Vesicles–Evidence of Unconventional Membrane Protein Orientation. Sci Rep 6:36338. https://doi.org/10.1038/srep36338
52. Bonsergent E et al (2021) Quantitative characterization of extracellular vesicle uptake and content delivery within mammalian cells. Nat Commun 12:1864. https://doi.org/10.1038/s41467-021-22126-y
53. Kang D, Oh S, Ahn S-M, Lee B-H, Moon MH (2008) Proteomic analysis of exosomes from human neural stem cells by flow field-flow fractionation and nanoflow liquid chromatography– tandem mass spectrometry. J Proteome Res 7:3475–3480
54. Lööv C, Scherzer CR, Hyman BT, Breakefield XO, Ingelsson M (2016) α-Synuclein in extracellular vesicles: functional implications and diagnostic opportunities. Cell Mol Neurobiol 36:437–448
55. Klein C, Schlossmacher MG, Parkinson (2007) disease, 10 years after its genetic revolution: multiple clues to a complex disorder. *Neurology* 69, 2093–2104
56. Chung YC, Kim SR, Jin BK (2010) Paroxetine prevents loss of nigrostriatal dopaminergic neurons by inhibiting brain inflammation and oxidative stress in an experimental model of Parkinson's disease. J Immunol 185:1230–1237
57. Scott DA et al (2010) A pathologic cascade leading to synaptic dysfunction in α-synuclein-induced neurodegeneration. J Neurosci 30:8083–8095
58. Soukup SF, Vanhauwaert R, Verstreken P (2018) Parkinson's disease: convergence on synaptic homeostasis. EMBO J 37:EMBJ201898960
59. Duda JE et al (2000) Immunohistochemical and biochemical studies demonstrate a distinct profile of α-synuclein permutations in multiple system atrophy. J Neuropathology Experimental Neurol 59:830–841
60. Kramer ML, Schulz-Schaeffer WJ (2007) Presynaptic α-synuclein aggregates, not Lewy bodies, cause neurodegeneration in dementia with Lewy bodies. J Neurosci 27:1405–1410
61. Volpicelli-Daley LA et al (2011) Exogenous α-synuclein fibrils induce Lewy body pathology leading to synaptic dysfunction and neuron death. Neuron 72:57–71
62. Heerssen HM, Pazyra MF, Segal RA (2004) Dynein motors transport activated Trks to promote survival of target-dependent neurons. Nat Neurosci 7:596–604
63. Chung CY, Koprich JB, Siddiqi H, Isacson O (2009) Dynamic changes in presynaptic and axonal transport proteins combined with striatal neuroinflammation precede dopaminergic neuronal loss in a rat model of AAV α-synucleinopathy. J Neurosci 29:3365–3373

64. Chu Y et al (2012) Alterations in axonal transport motor proteins in sporadic and experimental Parkinson’s disease. Brain 135:2058–2073
65. Volpicelli-Daley LA et al (2014) Formation of α-synuclein Lewy neurite–like aggregates in axons impedes the transport of distinct endosomes. Mol Biol Cell 25:4010–4023
66. Recasens A, Dehay B (2014) Alpha-synuclein spreading in Parkinson’s disease. Front Neuroanat 8:159
67. Emmanouilidou E et al (2016) GABA transmission via ATP-dependent K+ channels regulates α-synuclein secretion in mouse striatum. Brain 139:871–890
68. Ejlerskov P et al (2013) Tubulin polymerization-promoting protein (TPPP/p25α) promotes unconventional secretion of α-synuclein through exophagy by impairing autophagosome-lysosome fusion. J Biol Chem 288:17313–17335
69. Yamada K, Iwatsubo T (2018) Extracellular α-synuclein levels are regulated by neuronal activity. Mol neurodegeneration 13:9
70. Minakaki G, Krainc D, Burbulla LF (2020) The convergence of alpha-synuclein, mitochondrial, and lysosomal pathways in vulnerability of midbrain dopaminergic neurons in Parkinson’s disease. Front Cell Dev Biology 8:580634
71. Xie YX et al (2022) Lysosomal exocytosis releases pathogenic α-synuclein species from neurons in synucleinopathy models. Nat Commun 13:4918
72. Verweij FJ et al (2022) ER membrane contact sites support endosomal small GTPase conversion for exosome secretion. J Cell Biol 221:e202112032
73. Mahmood A et al (2023) Exosome secretion kinetics are controlled by temperature. Biophys J 122:1301–1314
74. Reyes JF et al (2014) Alpha-synuclein transfers from neurons to oligodendrocytes. Glia 62:387–398
75. Sengupta U et al (2020) Polymorphic α-synuclein strains modified by dopamine and docosahexaenoic acid interact differentially with tau protein. Mol Neurobiol 57:2741–2765
76. Konno M et al (2012) Suppression of dynamin GTPase decreases α-synuclein uptake by neuronal and oligodendroglial cells: a potent therapeutic target for synucleinopathy. Mol neurodegeneration 7:38
77. Fares M-B et al (2014) The novel Parkinson's disease linked mutation G51D attenuates in vitro aggregation and membrane binding of α-synuclein, and enhances its secretion and nuclear localization in cells. Hum Mol Genet 23:4491–4509
78. Karpowicz RJ Jr et al (2017) Selective imaging of internalized proteopathic α-synuclein seeds in primary neurons reveals mechanistic insight into transmission of synucleinopathies. J Biol Chem 292:13482–13497
79. Stuendl A et al (2016) Induction of α-synuclein aggregate formation by CSF exosomes from patients with Parkinson’s disease and dementia with Lewy bodies. Brain 139:481–494

80. Grey M et al (2015) Acceleration of α-synuclein aggregation by exosomes. J Biol Chem 290:2969–2982
81. Joensuu M et al (2017) Visualizing endocytic recycling and trafficking in live neurons by subdiffractional tracking of internalized molecules. Nat Protoc 12:2590–2622
82. Chai YJ et al (2016) Munc18-1 is a molecular chaperone for α-synuclein, controlling its self-replicating aggregation. J Cell Biol 214:705–718
83. Gormal RS et al (2020) Modular transient nanoclustering of activated β2-adrenergic receptors revealed by single-molecule tracking of conformation-specific nanobodies. *Proceedings of the National Academy of Sciences* 117, 30476–30487
84. Ershov D et al (2022) TrackMate 7: integrating state-of-the-art segmentation algorithms into tracking pipelines. Nat Methods 19:829–832. https://doi.org/10.1038/s41592-022-01507-1
85. Shrirao AB et al (2018) Microfluidic platforms for the study of neuronal injury in vitro. Biotechnol Bioeng 115:815–830
86. Wallis TP et al (2023) Super-resolved trajectory-derived nanoclustering analysis using spatiotemporal indexing. Nat Commun 14:3353

Figures

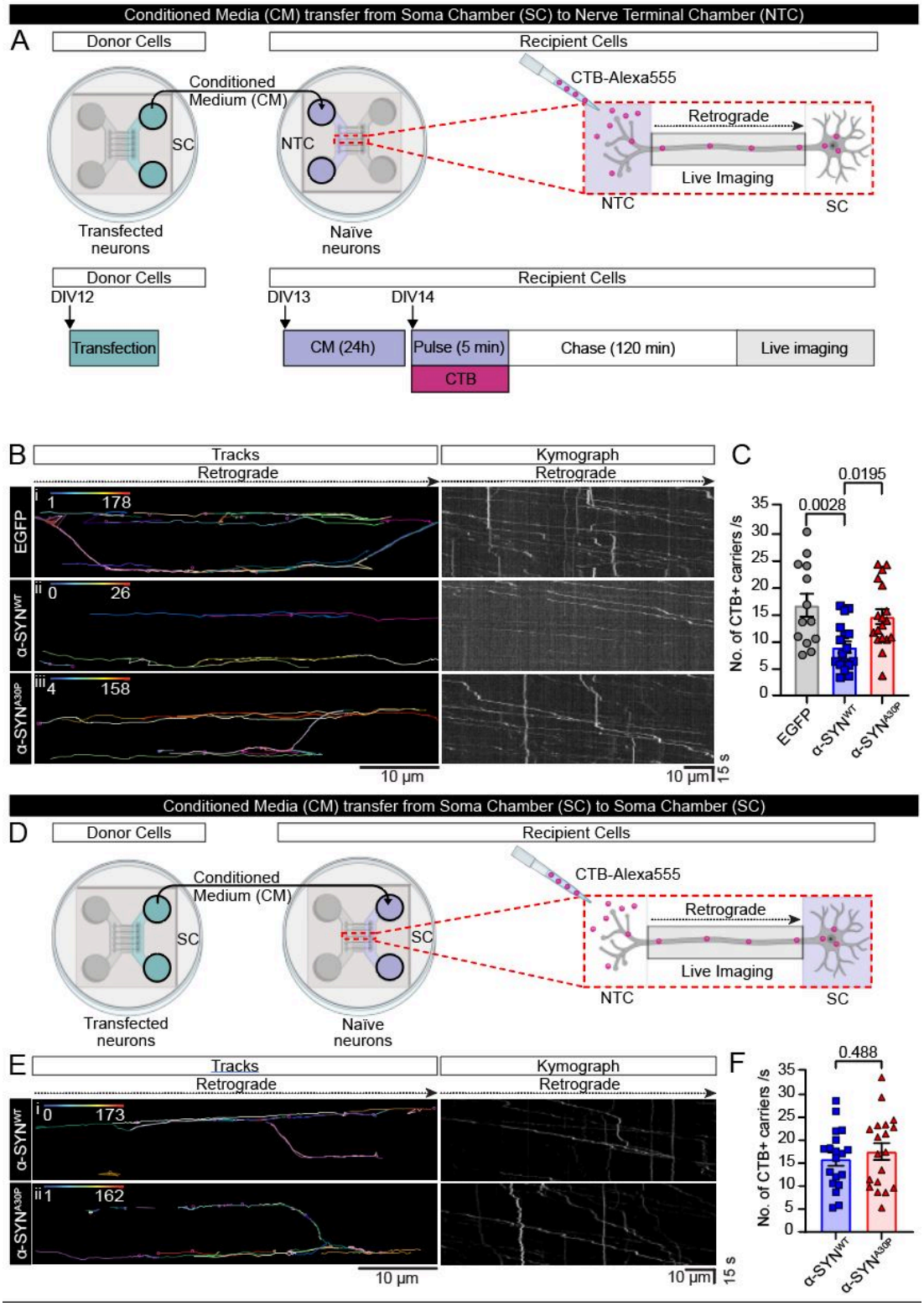


Figure 1

Conditioned medium from α-syn^{WT}-expressing neurons selectively reduces retrograde transport of CTB-positive carriers in recipient axons. (**A**) Schematic of the experimental design for conditioned medium (CM) transfer from the soma chamber (SC) of donor microfluidic devices to the nerve terminal chamber (NTC) of recipient devices. Primary hippocampal neurons from E16 mouse embryos were transfected at DIV12 with EGFP, α-syn^{WT}-GFP, or α-syn^{A30P}-GFP. After 24 h, CM from the donor SC was

transferred to the recipient NTC (70:30 vol/vol ratio). Recipient neurons were incubated with CM for 24 h, pulsed with CTB-Af555 (50 ng ml^{-1}) in high-K^+ buffer (56 mM) for 5 min, washed three times with low-K^+ buffer (5.6 mM), and chased for 2 h in CM before live imaging of retrogradely transported CTB-positive carriers. Time-lapse spinning-disk confocal imaging was performed at 3 Hz. (**B**) Representative track reconstructions and corresponding kymographs of retrogradely moving CTB-positive carriers in recipient axons exposed to CM from i, EGFP, ii, α-syn^{WT}-GFP, or iii, α-syn^{A30P}-GFP donor neurons. Left, TrackMate-based trajectories; right, corresponding kymographs. Scale bars, 10 μm (tracks) and 10 μm, 15 s (kymographs). (**C**) Quantification of CTB-positive carrier frequency in recipient axons following CM transfer to the NTC. Data are from 2 independent experiments with n = 13–18 microchannels per condition and are shown as mean ± SEM. Statistical analysis by one-way ANOVA with Tukey's multiple-comparison test. (**D**) Schematic of the control experiment in which CM from the donor SC was transferred to the recipient rather than the NTC. (**E**) Representative track reconstructions and kymographs of recipient axons exposed to CM from i, α-syn^{WT}-GFP or ii, α-syn^{A30P}-GFP donor neurons applied to the recipient SC. Scale bars, 10 μm (tracks) and 10 μm, 15 s (kymographs). (**F**) Quantification of CTB-positive carrier frequency following CM transfer to the recipient SC. Data are from 2 independent experiments with n = 19 microchannels and are shown as mean ± SEM. Statistical analysis by two-tailed unpaired Student's t-test.

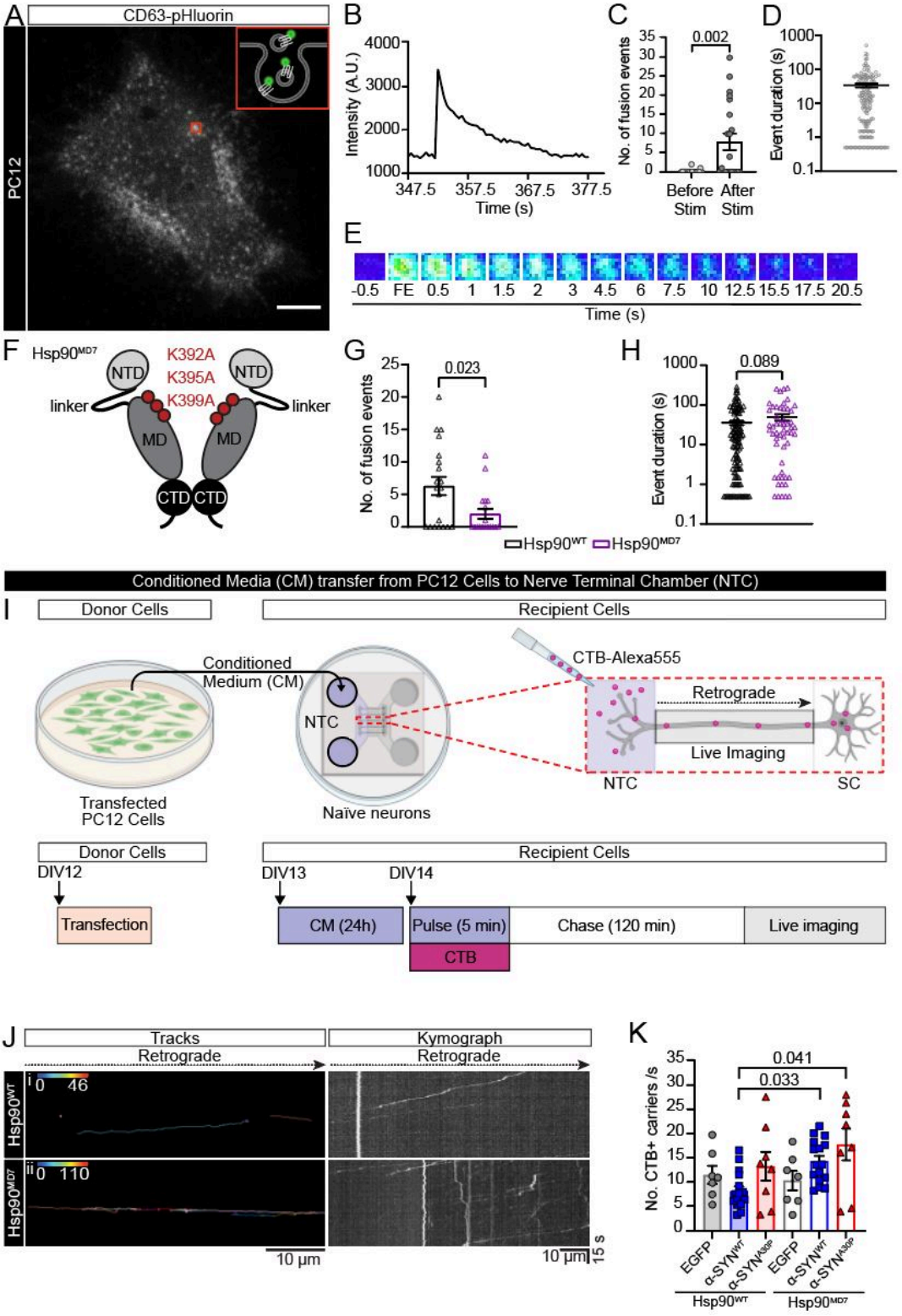


Figure 2

Hsp90-dependent EV release is required for α-syn-mediated disruption of retrograde transport. PC12 cells were co-transfected with an EV marker (CD63-pHluorin) and with either mCherry, Hsp90^{WT}-mCherry or mutant Hsp90^{MD7}-mCherry. 48 h post transfection, TIRF imaging of EV release was performed at 2 Hz on a Roper-iLas 2 microscope. A 10-minute timelapse was recorded with stimulation after 5 minutes using 2 mM barium chloride. (**A**) Representative TIRF image of a PC12 cell expressing CD63-pHluorin,

showing an individual exocytic event (red box). Scale bar, 10 μm. (**B**) Fluorescence intensity trace of the exocytic event shown in A. (**C**) Quantification of CD63-pHluorin fusion events detected before and after stimulation with 2 mM $BaCl_2$ in PC12 cells co-transfected with CD63-pHluorin and mCherry. Data are from 4 independent experiments with n = 21 cells and are shown as mean ± SEM. Statistical analysis by two-tailed Wilcoxon matched-pairs test. (**D**) Duration of CD63-pHluorin exocytic events in PC12 cells co-transfected with mCherry. Data are from 4 independent experiments with n = 21 cells. (**E**) Time series of the representative exocytic event in A, aligned to fusion onset (fusion event; FE). (**F**) Schematic of the $Hsp90^{MD7}$ mutant showing substitutions in the amphipathic helix. (**G**) Quantification of CD63-pHluorin fusion events in PC12 cells co-transfected with either $Hsp90^{WT}$-mCherry or $Hsp90^{MD7}$-mCherry. Data are from 4 independent experiments with n = 17–19 cells and are shown as mean ± SEM. Statistical analysis by two-tailed Mann–Whitney test. (**H**) Duration of CD63-pHluorin exocytic events in cells expressing $Hsp90^{WT}$ or $Hsp90^{MD7}$. Data are from 4 independent experiments with n = 17–19 cells. Statistical analysis by two-tailed Mann–Whitney test. (**I**) Experimental workflow. PC12 cells were co-transfected with $Hsp90^{WT}$-mCherry or $Hsp90^{MD7}$-mCherry together with EGFP, α-syn^{WT}-GFP, or α-syn^{A30P}-GFP. After 24 h, conditioned medium was transferred to the nerve terminal chamber (NTC) of recipient hippocampal neurons cultured in microfluidic devices. Recipient axons were pulsed with CTB-Af555 (50 ng ml^{-1}), washed, chased for 2 h in conditioned medium, and imaged for retrograde transport. (**J**) Representative TrackMate reconstructions and corresponding kymographs of retrogradely transported CTB-positive carriers in recipient axons exposed to conditioned medium from donor PC12 cells expressing i, α-syn^{WT} + $Hsp90^{WT}$ or ii, α-syn^{WT} + $Hsp90^{MD7}$. Scale bars, 10 μm (tracks) and 10 μm, 15 s (kymographs). (**K**) Quantification of CTB-positive carrier frequency in recipient axons after conditioned medium transfer from the indicated donor PC12 cells. Data are from 2 independent experiments with n = 7–18 microchannels per condition and are shown as mean ± SEM. Statistical analysis by Kruskal–Wallis test.

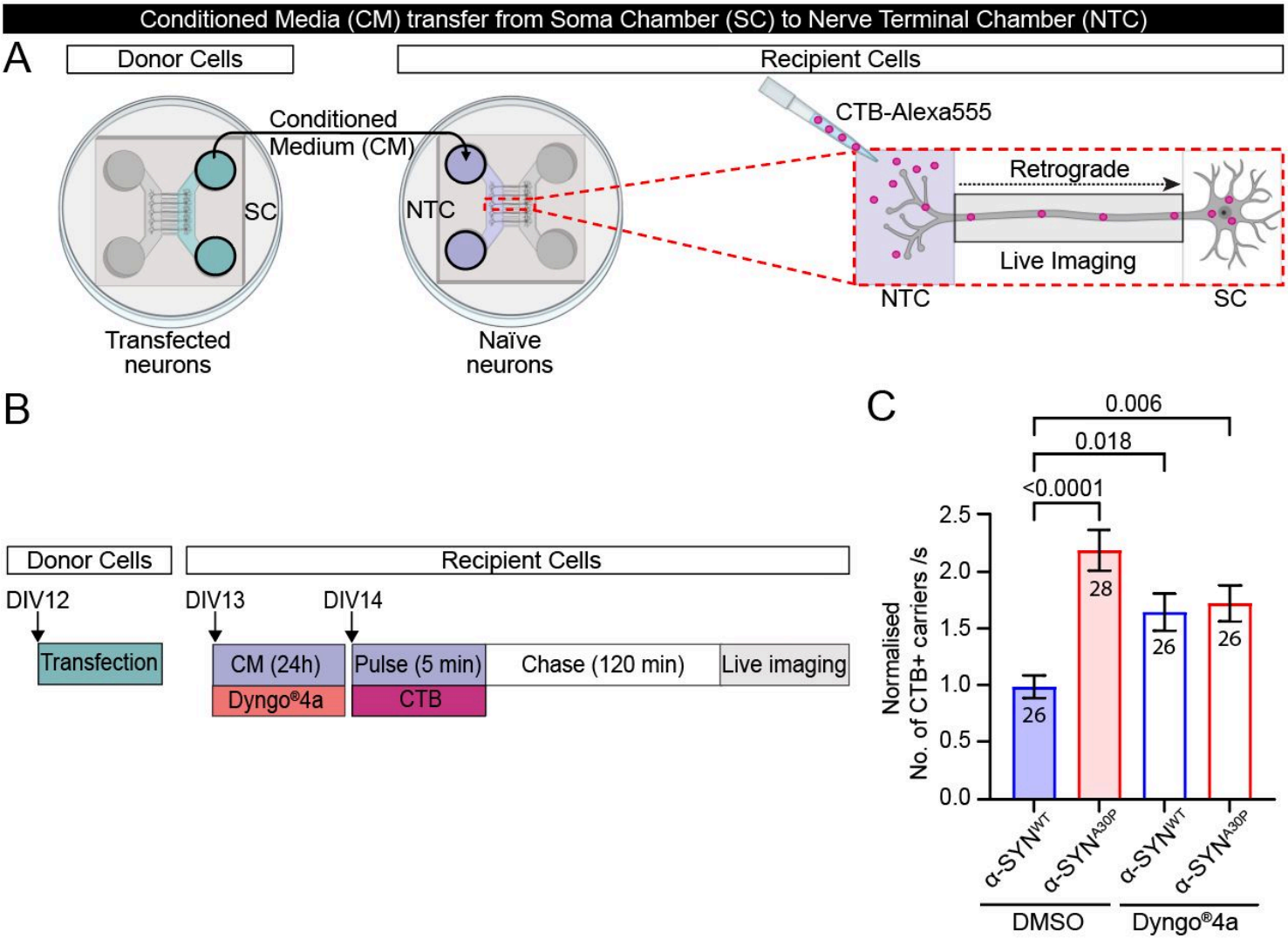


Figure 3

The downregulating effect of the conditioned medium in recipient neurons is dependent on endocytosis. (**A-B**) Schematic of the experimental paradigm: Microfluidic chambers were seeded with hippocampal neurons extracted from brains of E16 mouse embryos and neurons from the soma chamber (SC) were transfected with either α-syn^{WT}-GFP or α-syn^{A30P}-GFP (donor device; DIV 12). After 24 h, the conditioned medium from the SC of the donor device was added to the nerve terminal chamber (NTC) (70:30 vol/vol ratio) of the recipient device containing untransfected naïve neurons, in the presence of either Dyngo®4a (30 µM) or DMSO. The following day, a 5-minute pulse with Cholera toxin subunit B conjugated to Alexa Fluor™ 555 (CTB-Af555; 50 ng/mL) diluted in high potassium (HK$^+$) buffer was conducted, followed by 3 washes with low potassium (LK$^+$) buffer to remove the excess of CTB. Devices were then incubated for 2 h at 37 °C with Dyngo®4a free-conditioned medium, before imaging CTB-positive carriers undergoing retrograde transport in the axons of the recipient neurons. Timelapse confocal imaging was performed on the Discovery spinning disk at a 3 Hz imaging rate. (**C**) Quantification of the number of CTB+ carriers. Data from 3 independent experiments, n=26-28 channels, one-way ANOVA followed by Tukey's multiple comparison test, mean ± SEM.

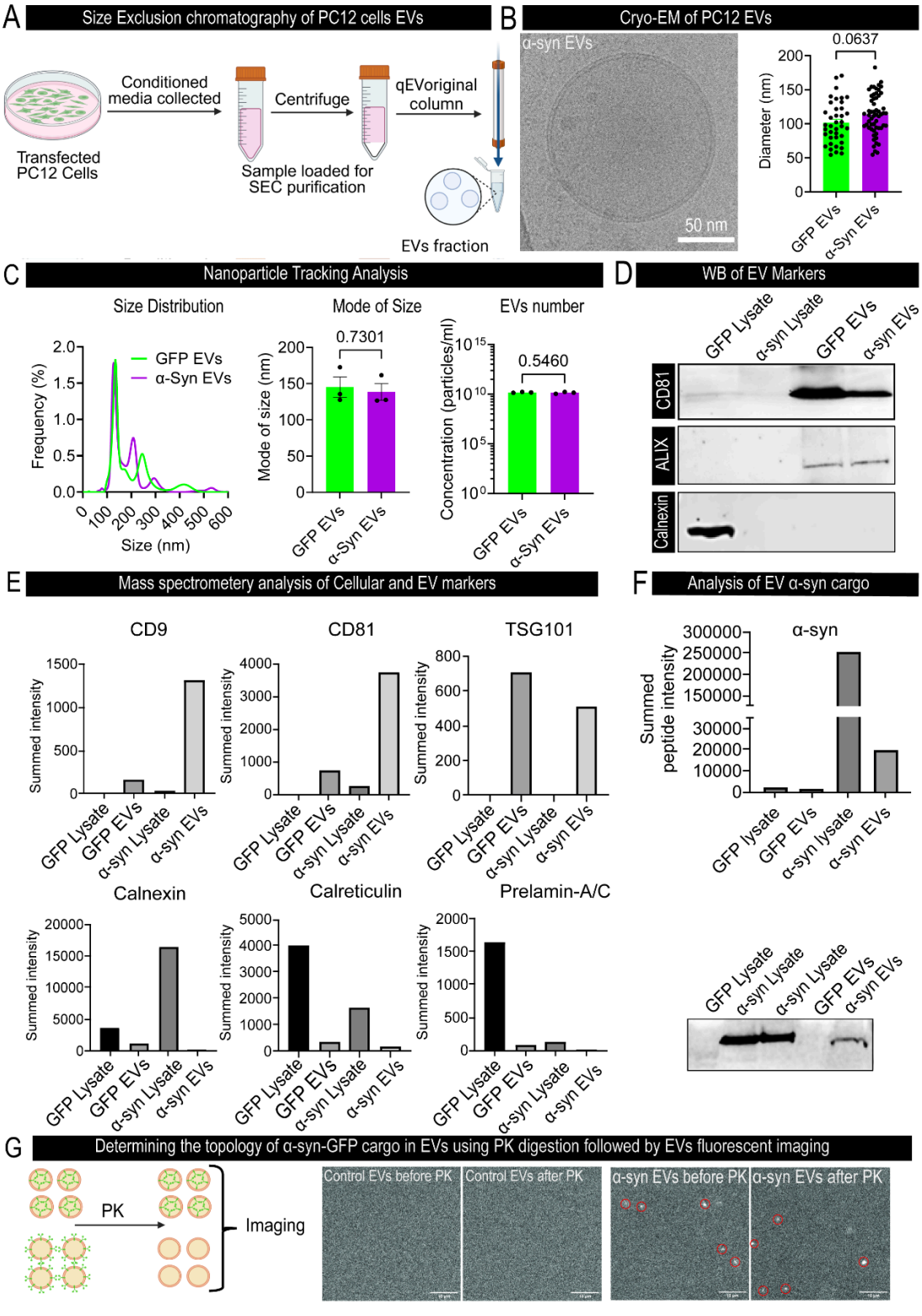


Figure 4

Isolation and characterization of extracellular vesicle (EV)-enriched fractions from GFP- or α-synuclein (α-syn)-expressing PC12 cells. (**A**) Schematic of EV isolation from conditioned medium of transfected PC12 cells by centrifugation followed by size-exclusion chromatography using a qEVoriginal column. (**B**)Representative cryo-electron micrograph of an EV from the α-syn EV preparation and quantification of vesicle diameter in GFP and α-syn EV fractions. Vesicle diameter was comparable between groups (P =

0.0637). Scale bar, 50 nm. (**C**) Nanoparticle tracking analysis of GFP and α-syn EV fractions showing particle size distribution (left), modal size (middle) and particle concentration (right). Modal size (P = 0.7301) and particle concentration (P = 0.5460) (n=4) were similar between groups. (**D**) Immunoblot analysis of matched cell lysates and EV fractions for the EV-associated proteins CD81 and ALIX and the endoplasmic reticulum marker calnexin. CD81 and ALIX were detected in EV fractions, whereas calnexin was not detected in EV fractions. (**E**) Mass spectrometry-based profiling of EV-associated and cellular proteins in GFP lysates, GFP EVs, α-syn lysates and α-syn EVs. EV-associated proteins (CD9, CD81 and TSG101) were detected in EV fractions, whereas cellular proteins (calnexin, calreticulin and prelamin-A/C) were enriched in lysates and depleted in EV fractions. Values are plotted as summed intensity. (**F**) α-Syn content in the same fractions measured by mass spectrometry (average peptide intensity; top) and immunoblotting (bottom). α-Syn was abundant in lysates from α-syn-expressing cells and detectable in the corresponding EV fraction but was not detected or was near background levels in GFP controls. (**G**) Single EV fluorescence imaging of pre and post Proteinase K digestion of α-syn-GFP and Control EV samples. Representative fluorescence microscopy images showing α-syn-GFP and Control EV samples pre and post Proteinase K digestion. GFP-positive EVs remained detectable in α-syn-GFP EV samples after Proteinase K treatment (red circles), suggesting that part of the GFP-associated α-synuclein signal is protected from protease digestion, either through localisation within intact EVs or within protease-inaccessible membrane-associated compartments. Negligible fluorescent particles were observed in the Control samples. Scale bars = 10 μm.

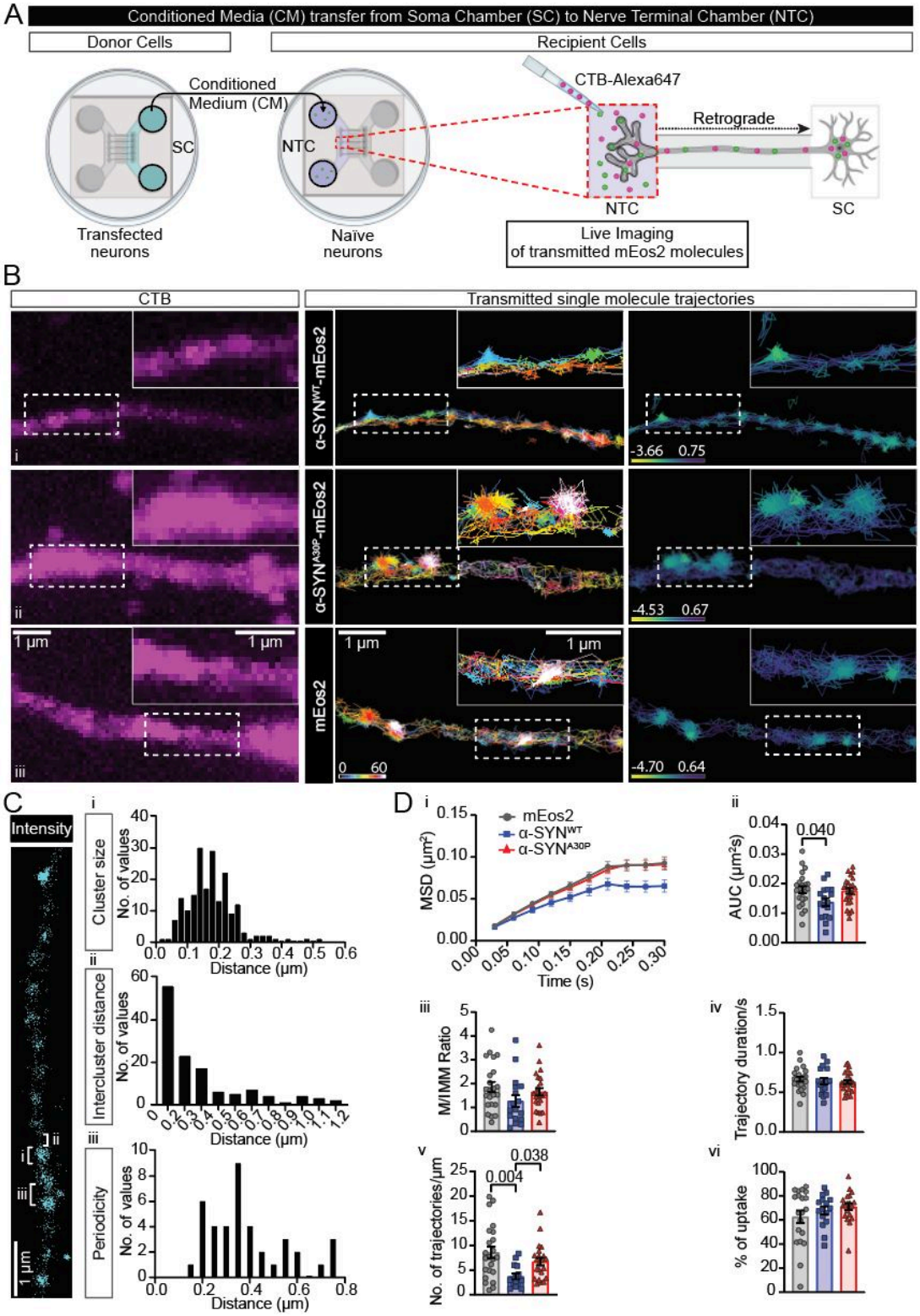


Figure 5

Single molecule imaging of transmitted α-syn in recipient neurons reveals distinct mobilities and a periodicity. (**A**) Detailed schematic of the experimental design: Microfluidic chambers were seeded with hippocampal neurons extracted from the brains of E16 mouse embryos and neurons from the soma chamber (SC) of the devices were transfected with either mEos2, α-syn^{WT}-mEos2 or α-syn^{A30P}-mEos2 (donor device; DIV 11-13). After 24 h, the conditioned medium from the SC of the donor device was

added to the nerve terminal chamber (NTC) (70:30 vol/vol ratio) of the recipient device containing untransfected naïve neurons. The following day, a 5-minute pulse with Cholera toxin subunit B conjugated to Alexa Fluor™ 647 (CTB-Af647; 50 ng/mL) diluted in high potassium (HK^+) buffer was conducted followed by three washes with low potassium (LK^+) buffer to remove the excess CTB. Devices were then incubated with the conditioned medium for 2 h at 37 °C before imaging CTB-positive carriers and mEos2 molecules undergoing retrograde transport in the axons of the recipient cells. Timelapse imaging was performed on the Elyra microscope. (**B**) Left panel, images of CTB-Af647 taken up by recipient neurons that were incubated with conditioned medium from neurons expressing i. α-syn^{WT}-mEos2, ii. α-syn^{A30P}-mEos2 or iii. mEos2 alone. PALMtracer was used to draw regions of interest (ROIs) around axons. Middle panel, sptPALM super-resolved trajectory images of either, i. α-syn^{WT}-mEos2, ii. α-syn^{A30P}-mEos2 or iii. mEos2 transferred to recipient neurons; the colour gradient of the calibration bar indicates the time of detection for trajectories (seconds): dark blue corresponds to a molecule detected at the beginning of acquisition and white corresponds to a molecule detected at the end of the acquisition. Right panel, super-resolved diffusion coefficient images generated using NASTIC software of either, i. α-syn^{WT}-mEos2, ii. α-syn^{A30P}-mEos2 or iii. mEos2 transferred to recipient neurons where each trajectory is coloured according to the value of the diffusion coefficient ($\log_{10}[\mu m^2 s^{-1}]$) for the first four time points. Yellow corresponds to molecules with lower mobilities (immobile) whilst dark blue corresponds to molecules with higher mobilities. Scale bar = 1 μm. (**C**) Periodicity analysis of α-syn^{WT}-mEos2 molecules in recipient neurons; analysis was carried out on intensity maps (left panel shows a representative image), scale bar = 1 μm, with analysis of i. α-syn^{WT}-mEos2 cluster size, ii. Distance between clusters and iii. Periodicity of clusters. (**D**) Mobility analysis of mEos2 molecules for all 3 conditions transferred to recipient neurons, i. Graph of the mean square displacement (MSD, μm^2), ii. Graph of the area under the MSD curve (AUC, $\mu m^2 s$), one-way ANOVA followed by Tukey's multiple comparison test, mean ± SEM. iii. Graph of the mobile/immobile ratio, Kruskal-Wallis test followed by Dunn's multiple comparison test, mean ± SEM iv. Graph of the duration of trajectories (seconds), one-way ANOVA followed by Tukey's multiple comparison test, mean ± SEM. v. Graph of the number of trajectories per μm, Kruskal-Walli's test followed by Dunn's multiple comparison test, mean ± SEM. Data from 10 independent experiments, n= 17-24 axons.

Supplementary Files

This is a list of supplementary files associated with this preprint. Click to download.

- EVaSynSupplemantryFigs.docx
- SIVideo1PrePostProtktreatmeetasynGFPControl1.mp4